Alma Mater Studiorum · Università di Bologna

Scuola di Scienze
Corso di Laurea Magistrale in Fisica

Quantum solitons in the XXZ model with staggered external magnetic field

Relatore:
Dr. Cristian Degli Esposti Boschi

Correlatore:
Prof. Elisa Ercolessi

Presentata da:
Luca Arceci

Sessione II
Anno Accademico 2013/2014

Abstract

La catena XXZ di spin 1/2 con campo magnetico esterno alternato, nel caso di campi abbastanza piccoli, può essere mappata in un modello di sine-Gordon quantistico tramite bosonizzazione: ciò assicura la presenza di eccitazioni di tipo solitone, antisolitone e breather. In particolare, l'azione del campo alternato apre un gap, così da rendere questi oggetti stabili contro fluttuazioni energetiche. Nel presente lavoro, questo modello è studiato sia analiticamente che numericamente. Inizialmente si svolgono calcoli analitici al fine di risolvere esattamente il modello tramite la tecnica di Bethe ansatz: si trova la soluzione per il modello XX + h alternato prima mediante trasformazione di Jordan-Wigner e poi con Bethe ansatz; si tenta successivamente di estendere quest'ultimo approccio al modello XXZ + h alternato, senza però trovare una soluzione esatta. Oltre a ciò, si calcolano le energie delle eccitazioni solitoniche elementari tramite DMRG (Gruppo di Rinormalizzazione della Matrice Densità) statico per diversi valori dei parametri nell'hamiltoniana. Si trova che i breathers compaiono nella regione antiferromagnetica, mentre solitoni ed antisolitoni sono presenti sia nella regione ferromagnetica che in quella antiferromagnetica. Si calcolano poi i loro valori di aspettazione della magnetizzazione di singolo sito lungo l'asse z, per vedere come appaiano in spazio reale. Si utilizza DMRG dipendente dal tempo per realizzare quenches sui parametri dell'hamiltoniana, al fine di monitorare l'evoluzione temporale di queste eccitazioni. I risultati ottenuti rivelano la natura quantistica di questi oggetti e forniscono informazioni riguardo le loro caratteristiche. Ulteriori studi sulle loro proprietà potrebbero portare alla realizzazione di stati a due livelli tramite una coppia solitone-antisolitone, al fine di implementare un bit quantistico.

Contents

Introduction

The investigation of the behaviour of quantum many-body systems is a very intriguing field of research: interactions in the quantum framework give rise to new peculiar phenomena and pave the way for new technological applications. In particular, quantum effects become more relevant when the system is confined in low dimensions: correlations between bodies are stronger and the behaviour of the system may show interesting features. Technological research is also moving in this direction: nanowires and nanodots, for example, promise to bring great further advancements, thanks to their peculiar properties due to quantum confinement.
However, this need for understanding quantum many-body systems has to face the problem of their great complexity. For the study of certain problems, classical computers seem to be no more adequate, since they are not able to store the huge amount of information these systems require. A possible solution to this problem could be the quantum computer, that is thought to be able to simulate quantum systems in a much more efficient way; in the last years, quantum information and computation, based on quantum bits (or qubits), have become two very hot fields of research.

This thesis work aims at localizing soliton excitations in a particular 1D magnetic model, to investigate the possibility of a new very intriguing way to realize a qubit on a solid-state environment through a soliton-antisoliton pair. Because of the soliton features, it would experience a weak coupling with the environment and hence would be less vulnerable to decoherence. This is an excellent quality for quantum information conveyance.
Besides, the model considered in this thesis might be realized experimentally by means of ultracold atoms. The spatial behaviour of quantum solitons has not been studied in depth yet, so observing it in condensed matter-like systems would be very interesting. The high-level of control and monitoring permitted by ultracold atoms technologies would make this objective possible.

This thesis provides an analytical and a numerical study of the 1D 1/2-spin XXZ model with staggered external magnetic field.
In the first chapter, an overview on classical solitons is given, with particular emphasis on the classical 1D sine-Gordon model and its solutions.
The second chapter introduces the magnetic model and, then, presents how it

may be mapped into the sine-Gordon model through the employment of the bosonization technique. This approach assures the presence of solitons in the magnetic model, but it is not particularly transparent in making contact with the lattice model.
Thus, in the third chapter, efforts to solve the model analytically through Bethe ansatz are explained. An interesting solution to the XX + h staggered model is given, while the same method applied to the XXZ + h staggered one fails.
Finally, the fourth chapter deals with the numerical study of the system through the Density Matrix Renormalization Group (DMRG) technique. The soliton excitation energies in the lowest part of the spectrum are pinpointed within numerical precision. Then, the behaviour of their magnetization is studied both in static and out of equilibrium conditions (by means of time-dependent DMRG).

Chapter 1

Solitary waves and solitons

Solitary waves and solitons are very peculiar physical phenomena that occur when dealing with non linear dispersive models. They are of particular interest both in pure and applied research and are employed in several fields such as quantum optics and condensed matter physics for example.
For the present work, two different kinds of solitons of the sine-Gordon model (namely the soliton and the antisoliton) will be used as the two states of a qubit. The aim is to convey information along an atomic chain with very little modification of the state of the qubit. Solitonic features are suitable for this purpose, since these objects can travel without changes for long distances.

In this chapter, an overview on solitary waves and solitons will be presented.
The first paragraph summarizes shortly the history of the soliton's discovery, from its first observation in nature by J. S. Russell to the early attempts to make it fit in the physical framework of the time.
The second paragraph is dedicated to the explanation of the concepts of solitary wave and soliton in classical physics. Moreover, some important models solved by solitons are presented.
The third paragraph presents in more detail the sine-Gordon model. It is of great importance in this work because, as we will see in the next chapter, the 1-D XXZ model with staggered external magnetic field can be mapped into a sine-Gordon model through bosonization.

1.1 Brief history of the soliton

The soliton is a physical phenomenon that was first observed in nature but was not previously predicted by any theory. Its first observation dates back to August 1834, when a naval engineer, Sir J. Scott Russell, saw by chance a strange kind of water wave travelling along a narrow channel: it was generated by the movement of boats docked in the channel and, as far as a human eye can tell, propagated without loosing its shape and with constant velocity. Russell followed that wave down the channel for a couple of miles on horseback and finally stopped and watched it go on without any appreciable energy dissipation. Here is what he wrote on his "Report on waves", a general review about waves, where he first discussed what he had called the "wave of translation":

I was observing the motion of a boat which was rapidly drawn along a narrow channel by a pair of horses, when the boat suddenly stopped - not so the mass of water in the channel which it had put in motion; it accumulated round the prow of the vessel in a state of violent agitation, then suddenly leaving it behind, rolled forward with great velocity, assuming the form of a large solitary elevation, a rounded, smooth and well-defined heap of water, which continued its course along the channel apparently without change of form or diminution of speed. I followed it on horseback, and overtook it still rolling on at a rate of some eight or nine miles an hour, preserving its original figure some thirty feet long and a foot to a foot and a half in height. Its height gradually diminished, and after a chase of one or two miles I lost it in the windings of the channel. Such, in the month of August 1834, was my first chance interview with that singular and beautiful phenomenon which I have called the Wave of Translation.

After this experience, Russell realized an experimental apparatus to reproduce the physical conditions for the generation of "waves of translation". He studied their features, finally determining that:

- The waves are stable and can travel over very large distances
- Their speed and width are respectively function of the size of the wave and the depth of the water
- Two or more different waves never merge
- If a wave is too big for the depth of the water, it splits into two of different size

However, Russell's wave of translation could not be described in terms of Newton's and Bernoulli's theories of hydrodynamics; only in the last decades of the 19^{th} century a first mathematical description of the phenomenon appeared in a paper published on "Philosophical Magazine" by Lord Rayleigh (inspired

by a previous work of J. Boussinesq).
Then, in 1895 D. Korteweg and G. de Vries published a paper where they wrote down a non linear partial differential equation that was solved by a wave of translation; this is the so-called KdV equation

$$\frac{du}{dt} + \frac{d^3u}{dx^3} - 6u\frac{du}{dx} = 0 \tag{1.1}$$

This is one of the most famous equations as regards soliton solutions.
In 1939 J. Frenkel and T. Kontorova found that another interesting model showed soliton solutions: it was the so-called sine-Gordon model, whose equation is:

$$\frac{d^2u}{dt^2} - \frac{d^2u}{dx^2} + \sin u = 0 \tag{1.2}$$

As we will see in one spatial dimension, this model has a rich variety of solutions: one of them, the breather, is a bound state of two different solitons and has a different behaviour in respect to the wave of translation observed by Russell.

1.1.1 A curious example: solitons in the Sulu Sea

Before we start to study the mathematical aspects of the subject, it is interesting to talk shortly about one manifestation of this peculiar phenomenon in nature.
In the early 80's travelling solitons have been individuated along the surface of the Sulu Sea, between Philippines and Borneo. They propagated over 400 km at a speed of 9 km/h, spreading radially from their place of formation. It is surprising to find them in such a huge environment, since Russell's waves of translation grew up in a narrow channel.
These waves tend to form near large submarine structures like a deep ocean sill or a continental shelf, because in these zones there are disruptions to the current flow. Some scholars believe a possible cause of this could be the tidal current.

A snapshot of the initial phase of formation of these waves is given in Fig. 1.1: the island of Pearl Bank is visible in the bottom of the image and, from this place, three different packets of solitons begin to move. Instead, Fig. 1.2 shows the propagation of one packet of solitons at a later stage, in a region of 60 km x 120 km.

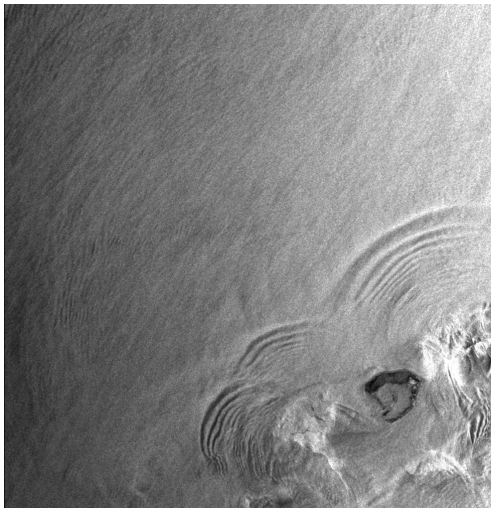

Figure 1.1: Early stage of formation of three different packets of solitons generated from Pearl Bank island (visible on the bottom right)

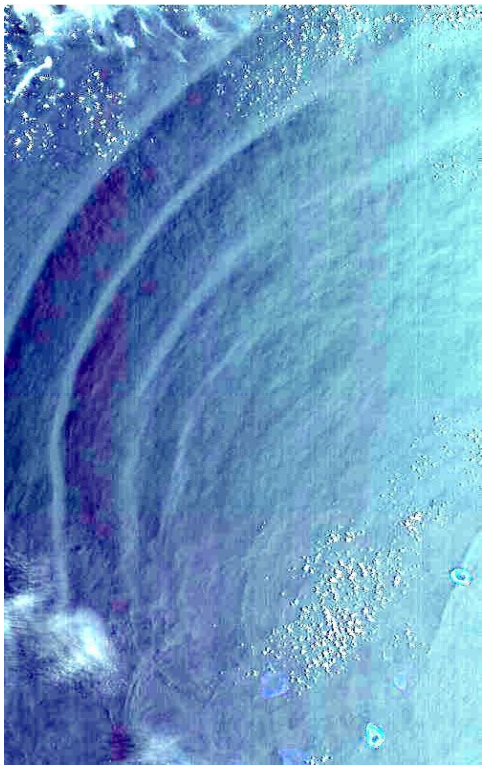

Figure 1.2: Solitons propagating over long distances from the islands of Bankoran and San Migel (on the bottom right): the image shows a portion of 60 km x 120 km of the Sulu Sea.

1.2 Definition of solitary wave and soliton

Progress in the mathematics and physics of waves of translation during the 20^{th} century showed that Russell's wave of translation is only a kind of a more general class of phenomena called solitons. In particular, two different but related classes of solutions of some specific non linear partial differential equations have been identified: the solitary wave and the soliton.
To define them, we will move in a classical physical framework and employ the energy density of the wave fields (solutions of differential field equations), following Rajaraman's dissertation in [5]. We are restricting ourselves to those field equations that have an energy density which is some function of the fields: $\epsilon(\phi_1, ..., \phi_i, ..., \phi_N, \vec{x}, t)$.
Therefore, a *solitary wave* is a field solution that has the following features:

$$\epsilon(\vec{x}, t) \quad localized\ in\ space \tag{1.3}$$

$$\epsilon(\vec{x}, t) = \epsilon(\vec{x} - \vec{v}t) \tag{1.4}$$

Condition 1.3 requires that the energy density should be finite in some finite region of space and that it should go to zero at infinity fast enough to be integrable. Its integral on the whole space yields the total energy of the system. Condition 1.4 means that the wave should propagate undistorted in shape and with constant speed. Note that any static localised solution is also a solitary wave, since this condition becomes an identity at any time.
Instead, a soliton is a solitary wave that shows an additional very peculiar feature: if two or more solitons start far apart and then collide in some region of space and time, after collision at $t \to +\infty$ they will have energy densities with same shapes and velocities as at $t \to -\infty$; the only things that could be changed by their interaction are their trajectories. In more formal terms, this implies the following conditions for the total energy density of a system of N solitons:

$$\begin{aligned} \epsilon(\vec{x}, t) &\to \sum_{i=1}^{N} \epsilon_0(\vec{x} - \vec{a}_i - \vec{v}_i t) \quad for\ t \to -\infty \\ \epsilon(\vec{x}, t) &\to \sum_{i=1}^{N} \epsilon_0(\vec{x} - \vec{a}_i - \vec{v}_i t + \vec{\delta}_i) \quad for\ t \to +\infty \end{aligned} \tag{1.5}$$

This is an amazing property, especially when it comes from non linear differential equations. The process of recreation of shape and velocity of the energy density profile is quite complex, and it is related to compensation effects between dispersion and non-linearity of the field equations.
To clarify this point (at least qualitatively), we start from a particular case of study: the model for a relativistic free wave field

$$\left(\frac{1}{c^2} \frac{\partial^2}{\partial t^2} - \frac{\partial^2}{\partial x^2} \right) \phi(x, t) = 0 \tag{1.6}$$

which is both linear and dispersionless. Any solution of this model can be written in the form

$$f(x - vt) = \int dk[a_1(k)\cos(kx - \omega t) + a_2(k)\sin(kx - \omega t)] \tag{1.7}$$

So, all the plane wave components of any solution have the same velocity $\omega/k = v$, and there are no dispersion effects. Moreover, wave packets experience no distortion in shape while travelling, hence they are solitary waves. Besides this, the wave equation is linear, therefore any linear combination of solutions is also a solution. We can then prepare the system as a linear combination of separate solitary waves and let them collide at a certain time; after scattering they will asymptotically tend to regain their original shapes and speeds.
This model, being dispersionless and linear, offers the simplest example of solitons. Nonetheless, as stated before, solitons usually emerge from non linear dispersive wave equations, where the situation is not so simple. We will try to explain qualitatively the mechanism of compensation through some considerations on the KdV equation.
Let's study first the dispersion effects getting rid of the non linear term

$$\frac{du}{dt} + \frac{d^3u}{dx^3} = 0 \tag{1.8}$$

Solutions to this equation are waves with a cubic dispersion relation $\omega = k^3$. Their phase velocities ($v_p = \omega/k$) and their group velocities ($v_g = \partial\omega/\partial k$) will be different, so their plain wave components will travel with different speeds and the shape of the wave packet will tend to change.
Let's turn on the non-linear effects; omitting the dispersive term we have

$$\frac{du}{dt} + u\frac{du}{dx} = 0 \tag{1.9}$$

Here all the solutions are fo the form $u(x,t) = f(x - vt)$. Such a function is characterized by the fact that the velocity of a point of constant displacement v is equal to that displacement. So, portions of the wave undergoing greater displacements move faster than those undergoing smaller displacements, and the shape of the wave changes while travelling.
When these two effects exactly cancel each other, solitary waves and solitons may appear, as shown in Fig. 1.3. However, note that the above discussion refers to the existence of solitary waves, but says nothing about solitons and what happens during collision.

As the mechanism behind the formation of solitary waves and solitons is complex, it is hard to identify them: only a few equations are known to be solved by these objects.
In any case, a soliton is much harder to find than a solitary wave. In fact,

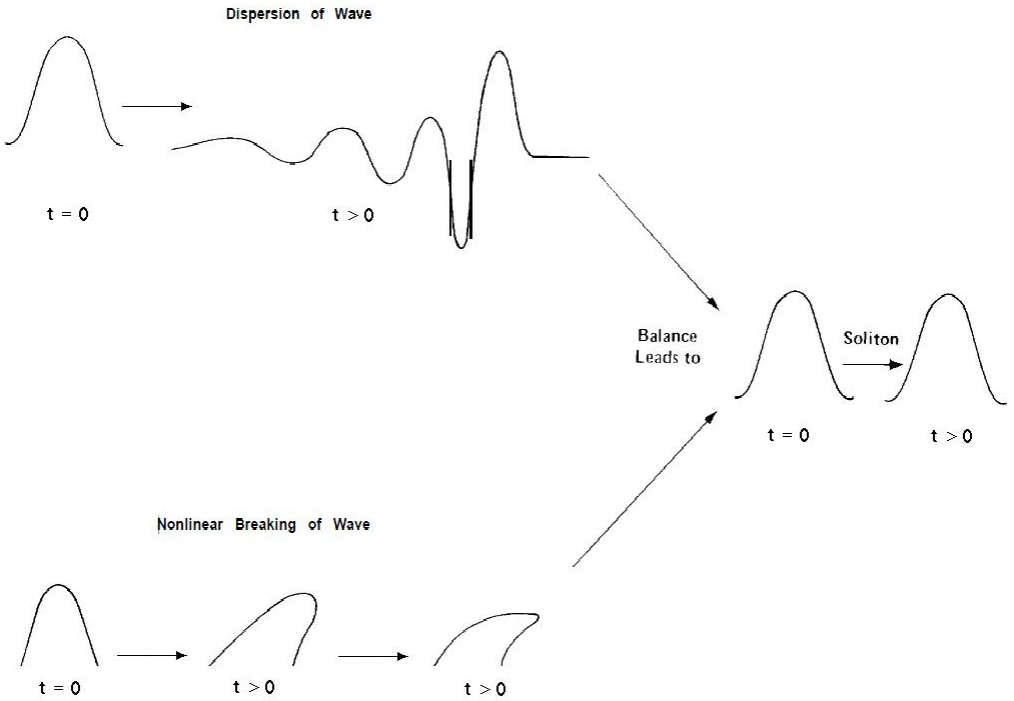

Figure 1.3: Qualitative representation of the compensation mechanism. Simultaneous modification of the wave packet due both to dispersion (top) and non-linearity (bottom) can leave the packet unchanged, forming a solitary wave or a soliton.

to verify that a solitary wave is also a soliton one has to take infinitely many time-dependent solutions consisting of an arbitrary number of solitons and check that condition 1.5 is satisfied.

Despite these two physical objects are clearly different, in the scientific literature they are often confused, and solitary waves are often called solitons even if condition 1.5 has not been verified.

We stress that this discussion deals with classical field equations: in the "quantum world" the definitions above have no meaning at all, so new arguments would be necessary.

1.3 Solitons in the 1D sine-Gordon model

Among the known wave field equations that exhibit soliton solutions, the sine-Gordon model is one of the most important and useful. It has been used in the study of a wide range of phenomena: propagation of crystal dislocations, of splay waves in membranes, of magnetic flux in Josephson lines, Bloch wall motion in magnetic crystals and two-dimensional models of elementary particles.

For this work's purposes, it assures the presence of soliton excitations in the XXZ model with staggered external magnetic field. In fact, as we will see in the next chapter, the latter model can be mapped into the sine-Gordon one through bosonization.

As we are interested in one-dimensional systems, we will study the 1-D sine-Gordon model; its Lagrangian density is

$$\mathcal{L}(x,t) = \frac{1}{2}(\partial_\mu \phi)(\partial^\mu \phi) + \frac{m^4}{\lambda}\left\{\cos\left[\frac{\sqrt{\lambda}}{m}\,\phi\right] - 1\right\} \tag{1.10}$$

where the relativistic notation is employed (∂_μ stands for space-time derivatives $\partial/\partial x^\mu$; x^μ is the space-time coordinate vector).

It is interesting to note that, in the limit of very small coupling constant $\lambda \to 0$, the Klein-Gordon equation is recovered.

The equation of motion can be obtained through the variational action principle applied to the Lagrangian. It turns out to be

$$\partial^\mu \partial_\mu \phi + \frac{m^3}{\sqrt{\lambda}} \sin\left[\frac{\sqrt{\lambda}}{m}\,\phi\right] = 0 \tag{1.11}$$

The reason why this model is so-called is now clear: its Lagrangian's form is similar to the Klein-Gordon model's one (they are equal in the limit of very small interaction), but a sine function appears in the equation of motion from the potential term.

The model can be brought in a clearer form by the substitutions $\tilde{x} = mx$,

$\tilde{t} = mt$ and $\tilde{\phi} = \frac{\sqrt{\lambda}}{m}\phi$; a simpler equation of motion appears:

$$\frac{\partial^2 \tilde{\phi}}{\partial \tilde{t}^2} - \frac{\partial^2 \tilde{\phi}}{\partial \tilde{x}^2} + \sin \tilde{\phi} = 0 \tag{1.12}$$

Two discrete symmetries can be easily found from the Lagrangian and equation of motion's invariances:

$$\tilde{\phi}(\tilde{x}, \tilde{t}) \to -\tilde{\phi}(\tilde{x}, \tilde{t}) \tag{1.13}$$

$$\tilde{\phi}(\tilde{x}, \tilde{t}) \to \tilde{\phi}(\tilde{x}, \tilde{t}) + 2n\pi, \qquad n \in Z \tag{1.14}$$

We can start analysing this model looking for static localised solutions, the simplest form of solitary waves. The integration of the equation of motion yields two different solutions, which we call the *soliton* and the *antisoliton* waves:

$$\tilde{\phi}_{sol}(x) = 4 \arctan \left[\exp(\tilde{x} - \tilde{x}_0)\right] \tag{1.15}$$

$$\tilde{\phi}_{antisol}(x) = -4 \arctan \left[\exp(\tilde{x} - \tilde{x}_0)\right] = -\tilde{\phi}_{sol}(x) \tag{1.16}$$

From Fig. 1.4 we can see that these fields are localised and their energy densities are localised too, so they are solitary waves. Their masses are the same and have the simple expression $M_{sol} = 8m^3/\lambda$.
If we are dealing with Galilean (or, in general, relativistic) invariance, a clever trick can be used to put them into motion to verify whether they are solitons or not: we transform the coordinate frame into a moving one, so that the previous static wave becomes time-dependent (with $u = v/c$):

$$\tilde{x} - \tilde{x}_0 \to \frac{\tilde{x} - \tilde{x}_0 - u\tilde{t}}{\sqrt{1 - u^2}} \tag{1.17}$$

As stated in the previous paragraph, to prove they are solitons it is necessary to find exact time-dependent solutions of the field equations, comprising an arbitrary number of these objects under collision. It is not easy, and several techniques have been developed in order to reach this purpose, such as the inverse scattering method and the Backlund transformations for example. Here we did not mention the way to obtain these solutions, but we limit to show the results only. Two remarkable time-dependent solutions are the *soliton-antisoliton*, *soliton-soliton* and *antisoliton-antisoliton* wave fields

$$\tilde{\phi}_{SA}(\tilde{x}, \tilde{t}) = 4 \arctan \left(\frac{\sinh(u\tilde{t}/\sqrt{1 - u^2}}{u \cosh(\tilde{x}/\sqrt{1 - u^2}} \right) \tag{1.18}$$

$$\tilde{\phi}_{SS}(\tilde{x}, \tilde{t}) = 4 \arctan \left(\frac{u \sinh(\tilde{x}/\sqrt{1 - u^2}}{\cosh(u\tilde{t}/\sqrt{1 - u^2}} \right) \tag{1.19}$$

and, for the symmetry 1.13

$$\tilde{\phi}_{AA}(\tilde{x}, \tilde{t}) = -\tilde{\phi}_{SS}(\tilde{x}, \tilde{t}) \tag{1.20}$$

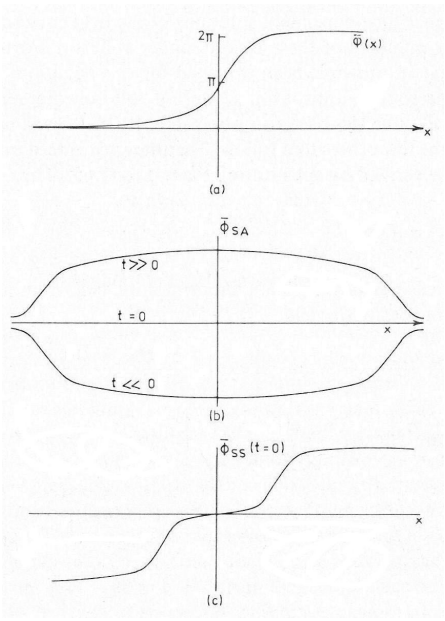

Figure 1.4: a) the static soliton (eq. 1.15 in real space; b) the soliton-antisoliton wave (eq. 1.18) at $t \to -\infty$, $t = 0$ and $t \to +\infty$; c) the soliton-soliton wave (eq. 1.19) at $t = 0$

It is interesting to see what happens to one of these solutions, say the soliton-antisoliton, in the limit of asymptotic behaviour

$$\begin{aligned}
\tilde{\phi}_{SA}(\tilde{x},\tilde{t}) &\to \tilde{\phi}_{sol}\left(\frac{\tilde{x}+u(\tilde{t}+\Delta/2)}{\sqrt{1-u^2}}\right)+\tilde{\phi}_{antisol}\left(\frac{\tilde{x}-u(\tilde{t}+\Delta/2)}{\sqrt{1-u^2}}\right) \quad t\to-\infty \\
\tilde{\phi}_{SA}(\tilde{x},\tilde{t}) &\to \tilde{\phi}_{sol}\left(\frac{\tilde{x}+u(\tilde{t}-\Delta/2)}{\sqrt{1-u^2}}\right)+\tilde{\phi}_{antisol}\left(\frac{\tilde{x}-u(\tilde{t}-\Delta/2)}{\sqrt{1-u^2}}\right) \quad t\to+\infty
\end{aligned} \tag{1.21}$$

with

$$\Delta \equiv \frac{1-u^2}{u}\ln u \tag{1.22}$$

This gives a concrete example of what was said before on the nature of solitons: initially $\tilde{\phi}_{SA}$ is made up of a soliton and an antisoliton moving towards each other; much after the collision, the scattering solution shows the same soliton-antisoliton pair, with the same shapes and speeds. The only residual effect due to the interaction appears as a time delay Δ. It is important to underline that, as we took $c = 1$ and $u = v/c$, then $u < 1$ and, consequently

$$\Delta < 0 \tag{1.23}$$

It means that a soliton and an antisoliton in collision proceed faster than u, the velocity they would have if they were not scattering. Hence, it seems like they experience an attractive force and speed up in each other's vicinity!

This is a remarkable result, linked to the existence of another different kind of soliton of the sine-Gordon model, namely the *breather* wave field. It is a particular bound state of a soliton and an antisoliton, and it can be obtained by putting a purely imaginary velocity $u = iv$ into eq. 1.18; what comes out is another real solution that has the form

$$\tilde{\phi}_{breather}(\tilde{x}, \tilde{t}) = 4 \arctan \left[\frac{\sin(v\tilde{t}/\sqrt{1+v^2})}{v \cosh(\tilde{x}/\sqrt{1+v^2})} \right] \tag{1.24}$$

Its form is very similar to the soliton-antisoliton one, but represents a completely different physical object. First of all, this is a periodic function with period $\tau = (2\pi\sqrt{1+v^2})/v$. This means that the soliton and the antisoliton oscillate about each other, remaining always close. It's a totally different picture from that of a soliton and an antisoliton getting farther and farther from each other after collision. Therefore, it is clear why this solution is called "breather": the shape of this wave stretches and shrinks periodically, remembering the two phases of a breathe.
Note that this is a time-dependent solution even if we have not Lorentz-transformed the reference frame yet. The two components move around the point $\tilde{x} = 0$ for every $\tilde{t}$. Hence, conditions for being a solitary wave are not automatically satisfied. It is possible to prove that this solution has localized and finite energy and that it is non-dispersive, but condition 1.4 does not hold in this case. However, in the rest frame the field remains confined within a definite static envelope, so we can think it as a soliton, although it does not satisfy all the conditions established before. This fact underlines the difficulty to find a definition that comprises all the possible cases of interest.

Let's turn our attention on the other two solutions ϕ_{SS} and ϕ_{AA}. It is possible to follow the same calculations as before and see that these wave fields simplify into two solitons (or two antisolitons) far apart, just as happens for ϕ_{SA}. However, what comes out is that the two solitons (or two antisolitons) colliding are subjected to a sort of repulsive force, hence they cannot form a bound state. If we put a purely imaginary speed in the expression for $\tilde{\phi}_{SS}$ (or ϕ_{AA}), the outcome is a complex function that cannot be admissible for a real scalar field system (like the one we are considering). So, a breather cannot be composed by two solitons or two antisolitons bound together.

Remembering definition 1.5, to prove that all these solitary waves are solitons we have to consider the scattering of an arbitrary number of solitons, antisolitons and breathers: after collision, they all have to asymptotically maintain their shapes and speeds. This demonstration can be carried out through the inverse scattering method, as in the works of Ablowitz et al. (1973) and Faddeev and collaborators (1974 and 1975). For our purposes, it suffices to know that this proof exists and that all the above wave fields behave as solitons.

Chapter 2

Bosonization of the 1D 1/2-spin XXZ + h staggered into the quantum sine-Gordon model

Bosonization is a powerful technique that can be applied to any 1D fermionic system with local hopping hamiltonian to map its particles into bosonic ones in the limit of small interactions. Its first formulation worked well in one spatial dimension only, but at a later stage efforts have been done to generalize it to higher dimensions [7].
As we will see, the XXZ model can be mapped into a fermionic hamiltonian through Jordan-Wigner transformation; so bosonization may be employed to investigate the lowest part of the energy spectrum. After calculations, one finds that the Jordan-Wigner spinless fermions of the XXZ model are converted into bosonic particles obeying a sine-Gordon hamiltonian. Since this latter model has soliton solutions, in some way the XXZ model would show the same kind of excitations too.
This is an interesting result but, if we want to realize stable excitations, it will not suffice. In fact, the XXZ model can be bosonized for values of the anisotropy between the ferromagnetic and antiferromagnetic points; however, in this region it is critical (i.e. gapless). Nonetheless, the addition of a staggered field opens a finite gap between the ground state and all the excitations. It can be shown that this model too can be mapped into a sine-Gordon one through bosonization: it will exhibit the soliton, the antisoliton and the breather in some region of space; this is exactly what we will be looking for in the following.

In the first paragraph of this chapter the Jordan-Wigner transformation is introduced and it is used to map the XXZ + h staggered model hamiltonian into the corresponding fermionic one.
The second paragraph presents the foundations of bosonization, from the lattice fermionic hamiltonian to the bosonic one and its continuum limit.

In the third paragraph bosonization is finally applied to the XXZ + h staggered hamiltonian, to show how the connection to the sine-Gordon model emerges.

2.1 From the spin to the fermionic picture: the Jordan-Wigner transformation

The model this work deals with is the 1-D 1/2-spin XXZ with the addition of a staggered external magnetic field. The hamiltonian is rather simple and has the form

$$H = -J \sum_{i=1}^{N} \left\{ S_i^x S_{i+1}^x + S_i^y S_{i+1}^y + \Delta S_i^z S_{i+1}^z \right\} + h \sum_{i=1}^{N} (-1)^i S_i^z \tag{2.1}$$

It is limited to nearest-neighbour interactions and the sums are over the N sites of the chain. It is important to note that the field and the anisotropy have the same direction along the z-axis: this is different from other more studied models where the staggered field is orthogonal to the anisotropy, for example the ones with Dzyaloshinskii-Moriya interaction.
An important feature of this hamiltonian is that it commutes with the total z-spin operator

$$[H, S_{tot}^z] = 0 \tag{2.2}$$

so that the total z-axis magnetization is a good conserved quantum number.
When the field is turned off, the 1/2-spin 1-D XXZ model is recovered. It has been well studied, and it is known to have three different phases as a function of J and Δ. When $J\Delta > 0$ and $|\Delta| > 1$, all the spins tend to arrange on the same direction and the phase is called *ferromagnetic*. On the contrary, when $J\Delta < 0$ and $|\Delta| > 1$ nearest-neighbour spins tend to have opposite direction in order to minimize the total energy; this is the *antiferromagnetic* phase. In both these regions excitations are gapped.
When $J\Delta \neq 0$ and $-1 < \Delta < 1$ configurations in the x-y plane energetically dominate those in the z-direction: this is the so-called *critical* region, since here the model is gapless (excitations take place in a continuum of energies without a gap). It is usually divided into two subregions: where $J\Delta > 0$ the phase is called ferromagnetic, while for $J\Delta < 0$ it is antiferromagnetic. These names mean that the spins tend to arrange more in one than in the other configuration, but this preferable configuration can be achieved in the limit of very strong coupling only. The distinction between these two subregions will be very important later, because the quantum breather will be found only in one of them.
Haldane's conjecture assures the validity of bosonization on this model only for parameter values within the critical region: hence, to obtain a gap it is necessary to introduce a staggered external field.

Eq. 2.1 can be rewritten in a more convenient form using the ladder spin operators

$$\begin{aligned} S^+ &= S^x + iS^y \\ S^- &= S^x - iS^y \end{aligned} \tag{2.3}$$

so that the hamiltonian becomes

$$H = -J \sum_{i=1}^{N} \left\{ \frac{1}{2} [S_i^+ S_{i+1}^- + S_i^- S_{i+1}^+] + \Delta S_i^z S_{i+1}^z \right\} + h \sum_{i=1}^{N} (-1)^i S_i^z \tag{2.4}$$

Operators 2.3 simply flip the z-spin up (S^+) or down (S^-), giving zero if the spin is already in the direction they want to bring it. Hence they correspond to a sort of kinetic term, because they tend to move the spins along the chain. The third is instead an interaction term, with the anisotropy quantifying the coupling between the bodies in the system.
Finally, the field acts as a one-body operator, contrasting the movement of spins and promoting their static behaviour.

It is now time to introduce the so-called Jordan-Wigner transformation, a clever trick that works with 1/2-spin chains only and maps the spin operators into spinless fermionic ones

$$\begin{cases} S_j^+ = \left[\prod_{i=1}^{j-1} (1 - 2n_i) \right] c_j \\ \\ S_j^- = \left[\prod_{i=1}^{j-1} (1 - 2n_i) \right] c_j^\dagger \\ \\ S_j^z = \frac{1}{2} (1 - 2n_j) \end{cases} \tag{2.5}$$

The effect of this transformation is to map a spin up into an empty state and a spin down into a particle. The operator in front of c_j takes into account the number of particles in the chain before the one to destroy (or create): it simply adds a minus sign when the number of particles is odd, but gives the identity operator in the even case. This is because spin operators commute, while fermionic ones anticommute.
Applying eq.s 2.5 into the hamiltonian 2.4 we obtain

$$\begin{aligned} H_{JW} = \sum_{j=1}^{N} \Bigg\{ & - \frac{J}{2} \left(c_j^\dagger c_{j+1} + c_{j+1}^\dagger c_j \right) - J\Delta \left(n_j - \frac{1}{2} \right) \left(n_{j+1} - \frac{1}{2} \right) + \\ & - h(-1)^j n_j \Bigg\} \end{aligned} \tag{2.6}$$

This is a 1-D fermionic hamiltonian and so it can be bosonized. Note that the conserved quantity has now become the number of particles, as $[H, \sum_i n_i] = 0$. To obtain the following form, however, we chose different boundary conditions depending on the number of particles in the model: when N is odd, we have periodic boundary conditions ($c_1 = c_{N+1}$), while when N is even we consider antiperiodic boundary conditions ($c_1 = -c_{N+1}$).

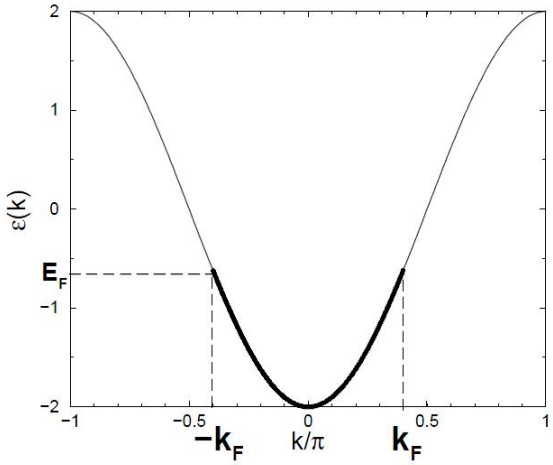

Figure 2.1: Dispersion relation for the XX model.

The choice of varying the boundary conditions depending on the number of particles permits to use always the same hamiltonian form; however, as a counterpart, it yields different quantization conditions (Fourier transforming the operators in the boundary condition equation)

$$\begin{aligned} k &= \frac{2n+1}{Na}\pi, \qquad n \in Z \\ k &= \frac{2n}{Na}\pi, \qquad n \in Z \end{aligned} \tag{2.7}$$

where a is the lattice constant. This choice is preferable since it is very useful to keep the same hamiltonian form in the following calculations.

2.2 Overview of bosonization

Let's consider first a free fermionic model, such the one obtained through eq. 2.6 putting $\Delta, h = 0$ (XX model). Particles do not interact and the energy spectrum can be very easily computed, after Fourier transforming the spinless fermionic operators. We avoid the straightforward calculations and show directly the result for the energies

$$\epsilon_k = -J \cos k \tag{2.8}$$

This dispersion relation is plotted in Fig. 2.1. When N particles are present, the ground state is populated by objects with momenta $|k| \leq k_F$, with k_F Fermi momentum. This is the so-called *non-interacting Fermi sea*, from which excitations may be stimulated.
Looking at Fig. 2.1 it is easy to see that, close to the Fermi momentum, there are two nearly linear regions. In the very weak coupling limit ($\Delta << J$),

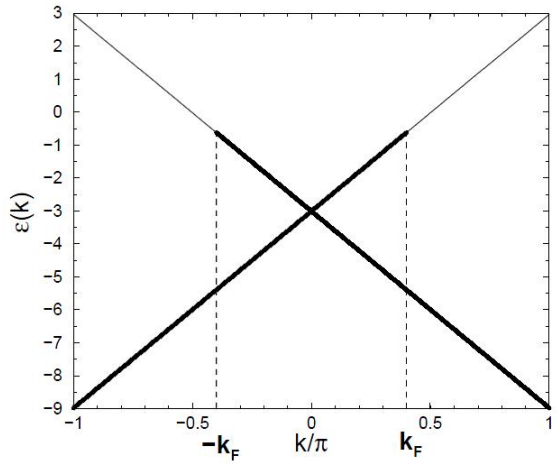

Figure 2.2: Dispersion relation for the linear dispersion model.

only the lowest energy states will be excited, so that particles will not move much further from the Fermi momentum. It is thus reasonable to linearise the spectrum around the two Fermi points (see Fig. 2.2), if interactions are low enough. Moreover, it is possible to mimic the continuum limit by extending the dispersion relation to infinity: this is the *linear dispersion model* and will be useful to explain bosonization.
The linear dispersion model presents two branches, named "left" and "right" because they refer to left and right-moving particles along the chain. We will analyse first what happens in one of them, namely the right one; then, we will extend the results to the other.

The first thing to define is how to span the Hilbert space of one branch of the linear dispersion model. The vacuum state is, by definition, the Fermi sea: it has all filled states for $k \leq k_F$ (Fig. 2.3a).
The hamiltonian conserves the number of particles, so it is useful to partition the Hilbert space with respect to it. However, because of the continuum limit, the number of particles is always infinite. Thus it is helpful to take into account the difference between the number of particles in a generic state and that in the vacuum state by defining a new operator

$$\hat{N} = \sum_k \left[c_k^\dagger c_k - \langle c_k^\dagger c_k \rangle_0 \right] = \sum_k : c_k^\dagger c_k : \tag{2.9}$$

where $: - :$ is the normal-ordering operation, that moves all the annihilation operators to the right and all the creation operators to the left.
Then, a sector of the Hilbert space is spanned by all the possible particle-hole excitations on the corresponding N-particle ground state. This is illustrated in Fig. 2.3b.

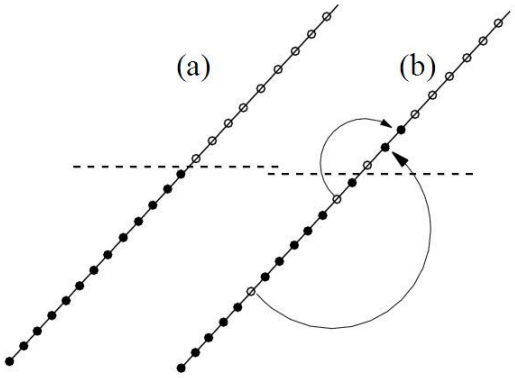

Figure 2.3: Schematic representation of the right branch of the dispersion relation a) in its vacuum state (Fermi sea) and b) for some particle-hole excitations.

We now want to find a way to express these fermionic operators in terms of other bosonic ones. The first step to do is the introduction of the density fluctuation operator

$$\rho_q \equiv \sum_k c^\dagger_{k+q} c_k \tag{2.10}$$

that creates a particular kind of particle-hole excitations: it enhances each particle momentum of q. The importance of this operator becomes evident when its commutator is calculated; it yields

$$[\rho(p), \rho(q)] = \frac{Lp}{2\pi}\delta_{p,-q} \tag{2.11}$$

It resembles a bosonic commutation relation and leads us to define a bosonic operator with the form

$$\begin{aligned} b_q &= \sqrt{\frac{2\pi}{Lq}}\rho(-q), \qquad q > 0 \\ b^\dagger_q &= \sqrt{\frac{2\pi}{Lq}}\rho(q), \qquad q > 0 \end{aligned} \tag{2.12}$$

They both commute with the operator in eq. 2.9 and so conserve the number of fermions. Moreover, it can easily be seen that

$$b_q|N\rangle_0 = 0, \quad \forall\, q,\, N \tag{2.13}$$

and this proves that the N-particle ground state contains no bosonic particle-hole excitations.
A relevant result, due to Haldane, proves that these bosonic operators span completely every subspace of the Hilbert space with fixed number of particles. So, a generic state with N fermions can be expressed as a function of $b^\dagger_q$

$$|N\rangle = f[\{b^\dagger_q\}]|N\rangle_0 \tag{2.14}$$

However, this does not suffice to substitute the action of the fermionic operators. b_q and $b_q^\dagger$ cannot change the number of fermions of a state, while c_q and $c_q^\dagger$ can. Therefore, new operators have to be introduced: the so-called Klein factors. Their action is to change the number of fermions by 1, leaving the particle-hole excitations unchanged

$$\begin{aligned} F^\dagger|N\rangle &= f[\{b_q^\dagger\}]|N+1\rangle_0 \\ F|N\rangle &= f[\{b_q^\dagger\}]|N-1\rangle_0 \end{aligned} \tag{2.15}$$

With both bosonic operators and Klein factors, it is finally possible to span the whole Hilbert space as if we were using the previous fermionic operators.

The next step is then to employ these results in the continuum limit. Let's introduce new field operators associated to the fermionic ones

$$\begin{aligned} \psi(x) &\equiv \frac{1}{\sqrt{L}} \sum_{k=-\infty}^{+\infty} e^{ikx} c_k \\ \psi^\dagger(x) &\equiv \frac{1}{\sqrt{L}} \sum_{k=-\infty}^{+\infty} e^{-ikx} c_k^\dagger \end{aligned} \tag{2.16}$$

The aim now is to find an expression of $\psi(x)$ in terms of bosons, $\hat{N}$ and Klein factors.
Firstly, an interesting information comes from calculating the commutator between the bosonic annihilation operator and fermionic field operator. In fact, this result can be used to derive the following relation

$$[b_q, \psi(x)]\,|N\rangle_0 = b_q\psi(x)|N\rangle_0 = \alpha_q\psi(x)|N\rangle_0 \tag{2.17}$$

Therefore, $\psi(x)|N\rangle_0$ is an eigenstate of b_q, with eigenvalue α_q (a function of q and x both). This means that this state is a *coherent state*, so it can be expressed in the usual form with an exponential operator acting on a vacuum state. Since $\psi(x)|N\rangle_0 \in H_{N-1}$, after some calculations this state may be expressed as

$$\psi(x)|N\rangle_0 = \frac{F}{\sqrt{L}} e^{i\frac{2\pi\hat{N}x}{L}} exp\left\{\sum_{q>0} \alpha_q(x) b_q^\dagger\right\}|N\rangle_0 \tag{2.18}$$

where the Klein lowering operator is introduced.
To generalize this result to an excited state $|N\rangle$, eq. 2.14 can be utilized. Going on with the calculus, the expression of the fermionic field as a function of bosons, $\hat{N}$ and Klein factors is found

$$\psi(x)|N\rangle = \frac{F}{\sqrt{L}} e^{i\frac{2\pi\hat{N}x}{L}} exp\left\{\sum_{q>0} \alpha_q(x) b_q^\dagger\right\} exp\left\{-\sum_{q>0} \alpha_q^*(x) b_q\right\}|N\rangle \tag{2.19}$$

Finally, bosonic field operators can also be introduced

$$\begin{aligned}\varphi_R(x) &= \frac{i}{\sqrt{L}}\sum_{q>0}\frac{e^{iqx}}{\sqrt{q}}e^{-\frac{\alpha q}{2}}b_q \\ \varphi_R^\dagger(x) &= -\frac{i}{\sqrt{L}}\sum_{q>0}\frac{e^{-iqx}}{\sqrt{q}}e^{-\frac{\alpha q}{2}}b_q^\dagger\end{aligned} \tag{2.20}$$

and a combination of them turns out to be particularly useful

$$\phi_R(x) = \varphi_R(x) + \varphi_R^\dagger(x) = \frac{i}{\sqrt{L}}\sum_{q>0}\frac{1}{\sqrt{q}}e^{-\frac{\alpha q}{2}}\left[e^{iqx}b_q - e^{-iqx}b_q^\dagger\right] \tag{2.21}$$

Through this latter definition, a direct relation between fermionic and bosonic fields can be found

$$\psi_R(x) = \frac{F}{\sqrt{2\pi\alpha}}e^{i\frac{2\pi\hat{N}x}{L}}exp\left[-i\sqrt{2\pi}\phi_R(x)\right] \tag{2.22}$$

We recall that all these results hold for the right-moving branch only. However, they can be easily extended to the left-moving one, taking into account the fact that all the completely filled states correspond to $k \geq -k_F$, while the empty ones to $k < -k_F$. By doing this, one finally obtains a fermionic field operator that is a combination of left and right-movers field operators

$$\psi(x) = e^{ik_Fx}\psi_R(x) + e^{-ik_Fx}\psi_L(x) \tag{2.23}$$

The same thing can be done for the bosonic fields; in particular, it is useful to define even and odd combinations of ϕ_R and ϕ_L

$$\begin{aligned}\phi(x) &= \frac{1}{\sqrt{2}}\left(\phi_L(x) - \phi_R(x)\right) \\ \theta(x) &= \frac{1}{\sqrt{2}}\left(\phi_L(x) + \phi_R(x)\right)\end{aligned} \tag{2.24}$$

and a canonical momentum field conjugate to ϕ

$$\Pi(x) = \partial_x\theta(x) \tag{2.25}$$

Now that all the most relevant bosonization relations have been shown, it is possible to apply them to the XXZ + h staggered model. This is next paragraph's issue.

2.3 Bosonization of the XXZ + h staggered model

The magnetic hamiltonian in eq. 2.4 is made of three terms: one kinetic, another of interactions between spins and the third of interaction of each spin

with the external field. We will examine them separately and eventually recombine the results.

Let's start with the free hamiltonian. Since there is no interaction, we will consider the linear dispersion model and take into account the right-moving branch only; the extension to the left one will be done at the end. In this model, energies are linearly proportional to the momenta, so that the hamiltonian can be written

$$H_J = v_F \sum_k k : c_k^\dagger c_k : \tag{2.26}$$

Calculating the commutator between H_J and $b_q^\dagger$, one then finds

$$H_J b_q^\dagger |N, E_N\rangle = (E_N + v_F q) b_q^\dagger |N, E_N\rangle \tag{2.27}$$

It is easy to see that the action of $b_q^\dagger$ on a generic state simply adds a bosonic quantum $v_F q$ to the total energy. Therefore, the only possible form for the hamiltonian in terms of bosonic operators may be

$$H_J = v_F \sum_{q>0} q b_q^\dagger b_q + E_0 \tag{2.28}$$

As can be seen making all the calculations, E_0 is inversely proportional to N, hence it goes to zero in the thermodynamic limit. Using the relations 2.16 one finally obtains an expression in terms of the fermionic fields. Adding the left-moving branch contribution, it is

$$H_J = v_F \int_{-\infty}^{+\infty} dx \left[: \psi_R^\dagger(x)(-i\partial_x)\psi_R(x) : + : \psi_L^\dagger(x)(i\partial_x)\psi_L(x) : \right] \tag{2.29}$$

It turns out to be useful to express this hamiltonian through the boson fields in eq.s 2.24 and 2.25

$$H_J = \frac{v_F}{2} \int dx \left[\Pi^2 + (\partial_x \phi)^2 \right] \tag{2.30}$$

As regards the interaction with the external field, recalling the third equation in 2.5 we can write

$$S_j^z \approx : \psi^\dagger(x)\psi(x) : \tag{2.31}$$

Using eq. 2.23 one can thus calculate an expression in terms of the right and left-field operators

$$S_j^z \approx : \psi_R^\dagger \psi_R : + : \psi_L^\dagger \psi_L : + e^{-2ik_F x} \psi_R^\dagger \psi_L + e^{2ik_F x} \psi_L^\dagger \psi_R == \rho(x) + (-1)^{\frac{x}{a}} M(x) \tag{2.32}$$

Low-energy excitations happen close to the Fermi points, so it follows that $e^{-2ik_F x} = e^{-i\pi x} = (-1)^j$. Moreover, two new operators have been introduced in the second equation: the uniform and the staggered single-site magnetization components

$$\rho(x) =: \psi_R^\dagger \psi_R : + : \psi_L^\dagger \psi_L : \tag{2.33}$$

$$M(x) =: \psi_R^\dagger \psi_L : + : \psi_L^\dagger \psi_R : \tag{2.34}$$

Therefore the single-site magnetization operator has a smooth and a rapidly oscillating part; the latter yields the so-called Umklapp terms, important for the generation of the periodic potential typical of the sine-Gordon hamiltonian. We now want to express the spin-spin interaction as a function of the fermionic fields. Thus, using eq.s 2.32, 2.33 and 2.34 we find

$$S_j^z S_{j+1}^z \approx: \rho(x)\rho(x+a) : -M(x)M(x+a) \tag{2.35}$$

where the second term creates some Umklapp interactions. The density operator play the role of a uniform single-site magnetization, while the other corresponds to a staggered magnetization (it exists independently from the external field). They can be expressed in terms of bosonic operators as

$$\rho(x) = \frac{1}{\sqrt{\pi}} \partial_x \phi(x) \tag{2.36}$$

$$M(x) \approx -\frac{1}{\pi a} : \sin\left(\sqrt{4\pi}\phi(x)\right) : \tag{2.37}$$

The $M(x)M(x+a)$ term in eq. 2.35 can be rewritten by expanding the operator product, so that one finally finds

$$M(x)M(x+a) \approx -\frac{1}{(\pi a)^2} \cos\left(\sqrt{16\pi}\phi(x)\right) - \frac{1}{\pi} \left(\partial_x \phi\right)^2 + const \tag{2.38}$$

As we said before, for this model bosonization holds for $|\Delta| < 1$ only. In this range of anisotropy, it turns out from renormalization group arguments that the cosine term is irrelevant. This means that, to describe the low-energy physics, we can neglect it and obtain a free bosonic hamiltonian (the so-called Luttinger liquid).
The remaining hamiltonian can then be rewritten as

$$H = \frac{u}{2} \int dx \left[K\Pi^2 + \frac{1}{K} (\partial_x \phi)^2 \right] \tag{2.39}$$

where K is the Luttinger parameter and u is the effective velocity. These two quantities can be exactly predicted for the XXZ model using the Bethe ansatz technique; they correspond to

$$K = \frac{\pi}{2 \arccos(\Delta)} \tag{2.40}$$

$$u = Ja \frac{\pi}{2} \frac{\sqrt{1-\Delta^2}}{\arccos(-\Delta)} \tag{2.41}$$

The hamiltonian in eq. 2.39 can be led to the canonical form by the scaling transformation

$$\phi(x) \to \sqrt{K}\phi(x), \qquad \Pi(x) \to \frac{1}{\sqrt{K}} \Pi(x) \tag{2.42}$$

All this work provides the bosonized hamiltonian for the XXZ model. The staggered external field term can be elaborated in the same way as before (calculations are simpler because it is a one-body operator); however, note that the uniform and staggered components in 2.32 are exchanged in this case, because of the effect of the staggered external field.
Working calculations out, one finally obtains

$$H_h \approx \frac{h}{\pi a} \sin(\sqrt{4\pi}\phi(x)) \tag{2.43}$$

This term is relevant, on the contrary of the previous one due to spin-spin interaction. Therefore, it provides a potential term of the sine-Gordon kind, even in the critical region.

In conclusion, bosonization for the XXZ + h staggered model yields the following hamiltonian

$$H_B = \int dx \left\{ \frac{u}{2} \left[\Pi^2 + (\partial_x \phi)^2 \right] - \frac{h}{\pi a} \sin(\sqrt{4\pi K}\phi) \right\} \tag{2.44}$$

It recalls the 1-D classical sine-Gordon model discussed in the previous chapter, even if here it is intended in a quantum framework. Therefore, we have just proved that there is a direct correspondence between this and the magnetic XXZ + h staggered model.
This means that, since there are soliton excitations in the quantum sine-Gordon model (as confirmed by the exact solution in the field-theoretic framework of the S-matrix), they will somehow have to be present in this magnetic model too.

The aim of this work is then firstly to pinpoint the energies of these excitations and then to understand how they behave in a condensed matter system.

Chapter 3

Analytical study of the XXZ + h staggered model

The XXZ model with staggered external magnetic field is in principle solvable through Bethe Ansatz techniques, although it is not straightforward to understand which ansatz should be adopted. However, such a solution would be of great interest for this work's purposes, since it would give information about all the possible excitations and would tell whether they are bound states or not. Thus, locating the breather would become very easy. Moreover, these exact results would assist the numerical ones, helping in their interpretation.
All these reasons motivate the efforts done to solve the model through the Bethe ansatz technique; unfortunately, as we will see, a complete solution is found for the XX + h staggered model only. Despite we do not get the exact solution in presence of z-spin interactions, the results obtained are useful anyway to understand the basic physics behind the model.
The strategy adopted is the following: firstly, calculate the solution of the XX + h staggered model through a different technique (the Jordan-Wigner transformation); using this result as a clue, find the correct ansatz that solves the same model; finally, use an identical ansatz to solve the model in presence of z-spin interactions. The idea that the ansatz should be the same for the XXZ + h staggered model comes from the fact that the same ansatz (the Bethe ansatz) solves both the XX and the XXZ model, even in presence of a uniform magnetic field. However, this initial assumption is probably wrong.

In this chapter, the first section is dedicated to the study of the XX + h staggered model by means of Jordan-Wigner transformation. Energies and eigenvalues are exactly calculated. Unfortunately, this technique cannot provide the solution of the XXZ model, but can help giving indications on the form of its eigenstates.
In the second paragraph the same model is analysed through a Bethe ansatz approach, obtaining the same results as before. Here we understand how to use this technique in presence of a staggered field.
Finally, in the third section the XXZ + h staggered model is studied using the

same ansatz as in the previous paragraph. Results and problems encountered are illustrated.

3.1 XX + h staggered model: Jordan-Wigner transformation

The Jordan-Wigner transformation is a useful and clever mathematical tool that maps a spin hamiltonian into a spinless fermionic one. We have already used it when dealing with bosonization, hence we refer to that section for its introduction and explanation.
Here the simplified XX + h staggered model is taken into account; its model hamiltonian in the spin picture is

$$H = -\frac{J}{2}\sum_{i=1}^{N}\left[S_i^+ S_{i+1}^- + S_i^- S_{i+1}^+\right] + h\sum_{i=1}^{N}(-1)^i S_i^z \tag{3.1}$$

where the upper S^+ and ladder S^- spin operators are introduced

$$\begin{aligned} S^+ &= S^x + iS^y \\ S^- &= S^x - iS^y \end{aligned} \tag{3.2}$$

In this study we take into consideration only an *even number of sites* for simplicity. To extend the calculations to the odd case, only slight changes should appear.
As said before, this spin-hamiltonian can be mapped into a spinless fermionic one through transformation 2.5. Neglecting constant energy terms, it looks

$$H = -\frac{J}{2}\sum_{i=1}^{N}\left[c_i^\dagger c_{i+1} + c_{i+1}^\dagger c_i\right] - h\sum_{i=1}^{N}(-1)^i c_i^\dagger c_i \tag{3.3}$$

where, in order to obtain the following expression, we have chosen *periodic boundary conditions* when the number M of particles is odd ($c_1 = c_{N+1}$), *antiperiodic boundary conditions* when M is even ($c_1 = -c_{N+1}$). This is because we have to take into account the fact that fermion operators anticommute, while spin operators commute. We stress the fact that the hamiltonian commutes with the S_{tot}^z operator, hence the total spin along the z-axis (i.e. the total particles number) is conserved.
Remembering the previous discussion in paragraph 2.1, this particular choice of boundary conditions yields different quantization conditions for M even and odd

$$\begin{aligned} k &= \frac{2n+1}{Na}\pi, \qquad n \in Z \\ k &= \frac{2n}{Na}\pi, \qquad n \in Z \end{aligned} \tag{3.4}$$

where a is the lattice constant.
Eq. 3.3 is a free hamiltonian, so the spinless fermions do not interact with each

other. The addition of the z-spin operators, instead, would bring a two-body operator in the fermionic picture, so that interactions emerge. This fact makes the process of diagonalization much harder, because a term with four different operators appears; this is why we do not solve the XXZ + h staggered model with this technique.
At this point, it is useful to move into the momentum space to underline better the features of the model; therefore, the coordinate space operators can be Fourier transformed as follows

$$\begin{aligned} c_j &= \frac{1}{\sqrt{N}} \sum_k e^{ikja} c_k \\ c_j^\dagger &= \frac{1}{\sqrt{N}} \sum_k e^{-ikja} c_k^\dagger \end{aligned} \tag{3.5}$$

to get the hamiltonian

$$H = \sum_{k \in [0, \frac{2\pi}{a}]} \Big\{ - J \ \cos(ka) c_k^\dagger c_k - h \ \ c_{k+\frac{\pi}{a}}^\dagger c_k \Big\} \tag{3.6}$$

The sum is over the first Brillouin zone and is of course restricted only to the discrete values allowed by the quantization condition. Note that the action of the staggered field is to introduce two operators that act on different momenta. It is thus convenient to split the first Brillouin zone in half, so that the hamiltonian can be written in the following form

$$H = \sum_{k \in [0, \frac{\pi}{a}]} \underbrace{\Big\{ - J \cos(ka) [c_k^\dagger c_k - c_{k+\frac{\pi}{a}}^\dagger c_{k+\frac{\pi}{a}}] - h [c_{k+\frac{\pi}{a}}^\dagger c_k + c_k^\dagger c_{k+\frac{\pi}{a}}] \Big\}}_{H_k} \tag{3.7}$$

The total hamiltonian is now divided into a sum of fixed-momentum hamiltonians; each of them can be written in a bilinear form, and the resulting matrix hamiltonian H_k can be easily diagonalized. Its eigenvalues are the possible energies of a particle with momentum k

$$E^\pm = \pm \sqrt{J^2 \cos^2(ka) + h^2} \tag{3.8}$$

There are two different energy bands in the split first Brillouin zone. They are specular and the opening of a gap of the order of h can be seen. It is important to note that the bands will not be filled by the spinless fermions directly, but by a linear combination of them generated by new operators that will be constructed in the following. Another important thing to note is that the ground state of the model do not correspond to its vacuum state: the lowest total energy is reached when the whole lower band is filled (it brings always negative energy) and the upper band is completely empty.
Now let's find the eigenstates related to the energies found above. To do this, a

rotation on the spinless fermionic operators can be made so that new operators appear

$$\begin{aligned}\eta_k &= \cos\theta_k c_k + \sin\theta_k c_{k+\frac{\pi}{a}} \\ \eta_{k+\frac{\pi}{a}} &= -\sin\theta_k c_k + \cos\theta_k c_{k+\frac{\pi}{a}}\end{aligned} \tag{3.9}$$

The expressions of the fermionic operators as a function of these new operators can now be put into the hamiltonian. Exact diagonalization is imposed by choosing the correct value of the angle θ_k (so that non-diagonal elements cancel); the result, without constant terms, is finally

$$H = \sum_{k\in[0,\frac{\pi}{a}]} \left[E^- \eta_k^\dagger \eta_k + E^+ \eta_{k+\frac{\pi}{a}}^\dagger \eta_{k+\frac{\pi}{a}}\right] \tag{3.10}$$

with the angle

$$\theta_k = \frac{1}{2}\arctan\frac{h}{J\cos(ka)} \tag{3.11}$$

Therefore, the first of these operators creates a quasi-particle with energy in the lower band; the other instead refers to the upper energy band.
All the eigenstates can in principle be built through these quasi-particle creation operators from the vacuum state (i.e. the state with all spin up). However, they do not give yet an explicit and clear expression in terms of fermionic operators in the real space. So, we now look for a general form for the eigenstates with fermionic operators in the lattice space.
We start with the ground state: as stated before, it corresponds to the state with all the possible particles in the lower band and the completely empty upper band

$$|GS\rangle = \prod_{k\in[0,\frac{\pi}{a}]} \eta_k^\dagger |0\rangle \tag{3.12}$$

When N is even, there will be $M = N/2$ particles; hence, the product is over all the $N/2$ values of the momenta in the first split Brillouin zone. To shift to the real space fermionic operators, we first substitute the operators in eq. 3.9 with the spinless fermionic ones in the momentum space and then Fourier antitransform; the result is

$$\begin{aligned}|GS\rangle &= \prod_{n=0}^{M-1}\left\{\frac{1}{\sqrt{N}}\sum_{j_n=1}^{N}\left[\underbrace{\left(\cos\theta_{k_n} + (-1)^{j_n-1}\sin\theta_{k_n}\right)e^{ik_n(j_n-1)a}}_{\alpha(j_n,k_n)} c_{j_n}^\dagger\right]\right\}|0\rangle = \\ &= \left(\frac{1}{N}\right)^{\frac{M}{2}}\prod_{n=0}^{M-1}\left[\alpha(1,k_n)\,c_1^\dagger \;+\; \alpha(2,k_n)\,c_2^\dagger \;+\; \ldots \;+\; \alpha(N,k_n)\,c_N^\dagger\right]\;|0\rangle\end{aligned} \tag{3.13}$$

This is a linear combination of N^M states, but many of them bring zero contribution: in fact, any time a fermionic operator is repeated at least twice, it gives zero because

$$(c_j^\dagger)^2 = 0 \tag{3.14}$$

Deleting these elements, $\frac{N!}{(N-M)!}$ states remain; however, they are not all orthogonal to all the others: there are several terms with the same fermionic operators that are arranged in a different order (for example, $c_j^\dagger c_l^\dagger c_k^\dagger$ and $c_l^\dagger c_k^\dagger c_j^\dagger$). Hence, they refer to the same state and can be brought to normal form simply by flipping the operators in agreement with the anticommutation relations. In doing this, particular attention has to be paid to the eventual minus sign due to an odd number of flips.
Finally, the number of independent states the ground state can be expressed with is

$$\frac{N!}{(N-M)!\,M!} = \binom{N}{M} \tag{3.15}$$

that is the actual dimension of the basis used. Each of its states can be univocally labelled by a ordered vector containing all the sites numbers the fermionic operators refer to; it is then convenient to define the ensemble ζ containing all the possible $\binom{N}{M}$ combinations of these vectors, so that the ground state can now be written as

$$|GS\rangle = \left(\frac{1}{N}\right)^{\frac{M}{2}} \sum_{\vec{x}\in\zeta} \Big\{ \sum_{P(M)} \alpha(\vec{x}(P(1)), k_0)\ \alpha(\vec{x}(P(2)), k_1)\ ... \\ ...\ \alpha(\vec{x}(P(M)), k_{M-1})\ sgn(P) \Big\}\ c^\dagger_{\vec{x}(1)} c^\dagger_{\vec{x}(2)} ... c^\dagger_{\vec{x}(M)}\ |0\rangle \tag{3.16}$$

In this form, $sgn(P)$ takes into account the number of flips done.
The ground state may now be excited (by annihilating some quasi-particles in the lower band and/or creating other quasi-particles in the upper one) and it is interesting to ask how such a state looks like.
Say that there are in general m quasi-particles in the upper band and $M-m$ quasi-particles in the lower band. In this case, we do not have to choose all the momenta in the first split Brillouin zone as for the ground state, but have some arbitrariness. It is thus convenient to introduce two ensembles A and B, containing all the momenta related respectively to the lower and the upper band

$$\begin{aligned} A &= \left\{ all\ the\ particles\ momenta\ k \ \mid\ k \leq \frac{\pi}{a} \right\} \\ B &= \left\{ all\ the\ particles\ momenta\ k \ \mid\ \frac{\pi}{a} \leq K \leq \frac{2\pi}{a} \right\} \end{aligned} \tag{3.17}$$

Therefore, a generic eigenstate is

$$
\begin{aligned}
|m, M-m\rangle &= \prod_{K\in B} \eta_K^\dagger \prod_{k\in A} \eta_k^\dagger \, |0\rangle = \\
&= \left(\frac{1}{N}\right)^{\frac{m}{2}} \prod_{K\in B} \Big[\sum_{j=1}^{N} \underbrace{\left(-\sin\theta_K + (-1)^{j-1}\cos\theta_K\right) \, e^{iK(j-1)a}}_{\beta(j,K)} \, c_j^\dagger \Big] \cdot \\
&\cdot \left(\frac{1}{N}\right)^{\frac{M-m}{2}} \prod_{k\in A} \Big[\sum_{j=1}^{N} \underbrace{\left(\cos\theta_k + (-1)^{j-1}\sin\theta_k\right) \, e^{ik(j-1)a}}_{\alpha(j,k)} \, c_j^\dagger \Big] |0\rangle
\end{aligned}
\tag{3.18}
$$

Hence, for each excitation in the upper (lower) band a β (α) coefficient contributes. Following the same reasoning as before, we then arrive to the general form of an eigenstate in the XX + h staggered model

$$
\begin{aligned}
|m, M-m\rangle = \left(\frac{1}{N}\right)^{\frac{M}{2}} \sum_{\vec{x}\in\zeta} \Big\{ \sum_{P(M)} & \beta(\vec{x}(P(1), B(1))) \dots \beta(\vec{x}(P(m), B(m))) \\
& \alpha(\vec{x}(P(m+1), A(1))) \dots \alpha(\vec{x}(P(M), A(M-m))) \\
& sgn(P) \Big\} \, c^\dagger_{\vec{x}(1)} c^\dagger_{\vec{x}(2)} \dots c^\dagger_{\vec{x}(M)} |0\rangle
\end{aligned}
\tag{3.19}
$$

What remains to do is to return to the spin picture, so that we will be able to compare these results with the ones deriving from the Bethe ansatz approach. For this purpose we use the Jordan-Wigner anti-transformation

$$
\begin{cases}
c_j = \Big[\prod_{i=1}^{j-1} (2 S_i^+ S_i^- - 1) \Big] S_j^+ \\
\\
c_j^\dagger = \Big[\prod_{i=1}^{j-1} (2 S_i^+ S_i^- - 1) \Big] S_j^-
\end{cases}
\tag{3.20}
$$

The fermionic vacuum corresponds to the ferromagnetic state with all spins up-aligned. The effect of the operator $c^\dagger_{\vec{x}(M)}$ on this state consists in lowering the $\vec{x}(M)$-th spin and to leave all the others up; the operators before $S^-_{\vec{x}(M)}$ simply account of the number of spin down before the $\vec{x}(M)$-th site, which are all up, so it brings a 1. The same thing holds for the operators on the other sites, since they are decreasingly ordered. From this follows that we can express the eigenstates simply substituting the fermionic operators with the spin ones

$$
\begin{aligned}
|m, M-m\rangle = \left(\frac{1}{N}\right)^{\frac{M}{2}} \sum_{\vec{x}\in\zeta} \Big\{ \sum_{P(M)} & \beta(\vec{x}(P(1), B(1))) \dots \beta(\vec{x}(P(m), B(m))) \\
& \alpha(\vec{x}(P(m+1), A(1))) \dots \alpha(\vec{x}(P(M), A(M-m))) \\
& sgn(P) \Big\} \, S^-_{\vec{x}(1)} S^-_{\vec{x}(2)} \dots S^-_{\vec{x}(M)} |0\rangle
\end{aligned}
\tag{3.21}
$$

All this analysis, as said before, is valid for the XX+h staggered model only. However, it gives the taste of what happens when a staggered field is applied: a gap opens up, the energy band is split into two different ones and the first Brillouin zone can also be divided in two. The eigenvalues are built as a linear combination of all possible states with a fixed number of spinless fermions; coefficients depend not only on the momentum of each particle, but also on the parity of the site under consideration.
These conclusions lead us to the calculation of the exact solution of the same model investigated above through the Bethe ansatz method. In fact, the ansatz will have to assume a form similar to the one in eq. 3.21. As we will see in the next paragraph, this is true and the solution we arrive to with $M = \{0, 1, 2\}$ is the same as the one just calculated.

3.2 XX + h staggered model: Bethe Ansatz approach

In this paragraph, the aim is to find a way to solve the XX + h staggered model through the Bethe ansatz approach. As stated before, the usual Bethe ansatz does not work and we will search a new form for the ansatz, taking inspiration from eq. 3.21.
It is important to underline that this hamiltonian conserves the total spin momentum along the z-axis, which is therefore a good quantum number and the hamiltonian can be divided into blocks. Hence, we can study separately sectors with fixed number of spin up and spin down. Here the number of spin down will be labelled by M, while the number of spin up will be $N - M$, in correspondence to what done before with the Jordan-Wigner transformation.

The sector $M = 0$ corresponds to the ferromagnetic state $|\uparrow\uparrow \dots \uparrow\rangle$, which is evidently an eigenstate. It gives no kinetic contributions to the energy and the effect of the staggered field brings zero energy, so the total energy is $E(M = 0) = 0$.

As for the sector $M = 1$, it is easy to see that we cannot proceed with the expansion in the plane waves basis (the usual Bethe ansatz) because of the effect of the staggered field. In fact, the second part of the hamiltonian acts in different ways on even and odd sites, so states with a spin down on an even or an odd site will have different energies. This issue suggests to formulate a more general form for the eigenstates, taking parity into account

$$|\psi\rangle = \sum_{\substack{j=1 \\ j\ odd}}^{N} \Big[f_D(j) S_j^- + f_P(j+1) S_{j+1}^- \Big] |\uparrow\uparrow \dots \uparrow\rangle \tag{3.22}$$

Practically we are dividing the chain in subunits, each containing two neighbouring sites. f_D and f_P are two different functions to be determined later;

their form is defined by the usual Bethe Ansatz

$$\begin{aligned} f_D(j) &= A_D\, e^{ikj} \\ f_P(j+1) &= A_P\, e^{ik(j+1)} \end{aligned} \tag{3.23}$$

where we have now two different coefficients instead of a unique constant as in the case of absent or uniform magnetic field.
The condition to be satisfied by $|\psi\rangle$ in order to be an eigenstate of H is

$$H|\psi\rangle = E|\psi\rangle \tag{3.24}$$

Calculating the equation, projecting separately on states where the spin is lowered respectively in a odd and in a even site and then using the ansatz 3.23, we finally obtain the system

$$\begin{cases} -\frac{J}{2}A_P\Big[1 + e^{-i2k}\Big] - A_D(E-h)e^{-ik} = 0 \\ -\frac{J}{2}A_D\Big[e^{-ik} + e^{ik}\Big] - A_P(E+h) = 0 \end{cases} \tag{3.25}$$

From the second equation in 3.25 follows

$$A_D = -A_P \frac{E+h}{J\cos k}, \qquad \cos k \neq 0 \tag{3.26}$$

Thus, substituting it into the first equation in 3.25, we arrive to the equation for the energies (valid for $\cos k = 0$ also)

$$E = \pm\sqrt{J^2\cos^2 k + h^2} \tag{3.27}$$

These are the same two bands found with Jordan-Wigner calculations, but we have no indication about the eigenstates they refer to; we expect however to find something similar to what obtained through operators of eq. 3.9.
Therefore, next step is to determine the ansatz coefficients: from eq. 3.26 two different equations can be obtained substituting the two values of energy in eq. 3.27

$$\frac{A_D}{A_P} = \pm\sqrt{1 + \frac{h^2}{J^2\cos^2 k}} - \frac{h}{J\cos k} \tag{3.28}$$

where the upper sign refers to the lower energy band, the lower sign to the upper energy band. Remembering definition 3.11 in the previous paragraph, this equation can be written as follows

$$\begin{aligned} \frac{A_D}{A_P} &= -\frac{E+h}{J\cos k} = \\ &= \pm\sqrt{1+\tan^2 2\theta_k} - \tan 2\theta_k = \\ &= \pm \mid \frac{1}{\cos 2\theta_k} \mid - \tan 2\theta_k = \\ &= \pm\frac{\cos\theta_k \mp \sin\theta_k}{\cos\theta_k \pm \sin\theta_k} \end{aligned} \tag{3.29}$$

to express the relation between the coefficients of odd and even sites. These two values refer to the two different energies, so there will be two different types of eigenstates, corresponding to the states created by operators $\eta_k^\dagger$ and $\eta_{k+\pi}^\dagger$ from Jordan-Wigner approach. Note that $\cos k > 0 \longrightarrow 2\theta_k \in [0, \frac{\pi}{2}[$ and so $\cos 2\theta_k > 0$, while $\cos k < 0 \longrightarrow 2\theta_k \in]-\frac{\pi}{2}, 0]$ and so $\cos 2\theta_k < 0$: this justifies the elimination of the absolute value during calculations. The remaining case, $\cos k = 0$, can be evaluated separately from the system 3.25 and brings $E = -h, A_D = 0$ for $k = \frac{\pi}{2}$ and $E = +h, A_P = 0$ for $k = \frac{3}{2}\pi$, coherently with the results obtained above.
Using this result, we can express the eigenstates leaving only one coefficient, which can be computed imposing the normalization condition $\langle\psi|\psi\rangle = 1$

$$\begin{aligned} |\psi^-\rangle = \frac{A_P}{\cos\theta_k + \sin\theta_k} \sum_{\substack{j=1 \\ j\ odd}}^{N} \Big[& (\cos\theta_k - \sin\theta_k) e^{ikj} S_j^- + \\ & + (\cos\theta_k + \sin\theta_k) e^{ik(j+1)} S_{j+1}^- \Big] |\uparrow\uparrow \dots \uparrow\rangle = \\ = \frac{1}{\sqrt{N}} \sum_{j=1}^{N} & \Big[(\cos\theta_k + (-1)^j \sin\theta_k) e^{ikj} S_j^- \Big] |\uparrow\uparrow \dots \uparrow\rangle \end{aligned} \tag{3.30}$$

$$\begin{aligned} |\psi^+\rangle = \frac{A_P}{\cos\theta_k - \sin\theta_k} \sum_{\substack{j=1 \\ j\ odd}}^{N} \Big[& -(\cos\theta_k + \sin\theta_k) e^{ikj} S_j^- + \\ & + (\cos\theta_k - \sin\theta_k) e^{ik(j+1)} S_{j+1}^- \Big] |\uparrow\uparrow \dots \uparrow\rangle = \\ = \frac{1}{\sqrt{N}} \sum_{j=1}^{N} & \Big[(-\sin\theta_k + (-1)^j \cos\theta_k) e^{ikj} S_j^- \Big] |\uparrow\uparrow \dots \uparrow\rangle \end{aligned} \tag{3.31}$$

Eq 3.30 expresses an eigenstate with energy in the lower band, while eq 3.31 refers to the upper band. The coefficients in front of the states are exactly the same found with Jordan-Wigner calculations, although here we followed a very different path.

Flipping two spins down, the sector $M = 2$ is reached. In this case the situation is more complex, because we have to consider separately states with both spins in odd sites, both in even sites or a spin in a odd and the other in a even site; in fact, the hamiltonian acts differently in each of these states. A

sufficiently general expression for the eigenstates is

$$
\begin{aligned}
|\psi\rangle = & \sum_{\substack{1\le n_1<n_2<N \\ n_1,n_2 \text{ odd}}} \Big\{ f_{DD}(n_1,n_2)|n_1,n_2\rangle + \\
& \qquad + \; f_{PP}(n_1+1,n_2+1)|n_1+1,n_2+1\rangle + \\
& \qquad + \; f_{DP}(n_1,n_2+1)|n_1,n_2+1\rangle \Big\} + \\
& + \sum_{\substack{1\le n_1<n_2<N-1 \\ n_1,n_2 \text{ odd}}} \Big\{ f_{PD}(n_1+1,n_2+2)|n_1+1,n_2+2\rangle \Big\} + \\
& + \sum_{\substack{1\le n<N \\ n \text{ odd}}} \Big[f_{DP}(n,n+1)|n,n+1\rangle \Big] + \\
& + \sum_{\substack{1\le n<N-1 \\ n \text{ odd}}} \Big[f_{PD}(n+1,n+2)|n+1,n+2\rangle \Big]
\end{aligned}
\tag{3.32}
$$

The last line contains states where down spins are on neighbouring sites, the other two show all other possibilities. Note also that the second (fourth) sum differs from the first (third) by only the fact that $n_2 \neq N-1$ ($n \neq N-1$); this is necessary to avoid repetition of states due to periodic boundary conditions. This form for the eigenstates permits an easier evaluation of the hamiltonian operator effect, as we want the relation 3.24 to be valid. After calculations, there are six different states to project on (let n_1 and n_2 be two odd values in the ranges specified by the sums in 3.32):

1. $|n_1, n_2\rangle \qquad n_2 > n_1 + 2$
2. $|n_1+1, n_2+1\rangle \qquad n_2 > n_1 + 2$
3. $|n_1, n_2+1\rangle \qquad n_2 > n_1$
4. $|n_1+1, n_2+2\rangle \qquad n_2 > n_1$
5. $|n_1, n_1+1\rangle$
6. $|n_1+1, n_1+2\rangle$

Hence there are six different equations, from which energies and eigenstates can be drawn. Now we use a modified Bethe Ansatz to express the four functions multiplying the states in 3.32: we recall the results in 3.30 and 3.31 for $M = 1$ and write

$$
\begin{cases}
f_{DD} = \frac{1}{N} A_{12}(1-)(2-) e^{i(k_1 n_1 + k_2 n_2)} + \frac{1}{N} A_{21}(1-)(2-) e^{i(k_1 n_2 + k_2 n_1)} \\
f_{PP} = \frac{1}{N} A_{12}(1+)(2+) e^{i(k_1 n_1 + k_2 n_2)} + \frac{1}{N} A_{21}(1+)(2+) e^{i(k_1 n_2 + k_2 n_1)} \\
f_{DP} = \frac{1}{N} A_{12}(1-)(2+) e^{i(k_1 n_1 + k_2 n_2)} + \frac{1}{N} A_{21}(1+)(2-) e^{i(k_1 n_2 + k_2 n_1)} \\
f_{PD} = \frac{1}{N} A_{12}(1+)(2-) e^{i(k_1 n_1 + k_2 n_2)} + \frac{1}{N} A_{21}(1-)(2+) e^{i(k_1 n_2 + k_2 n_1)}
\end{cases}
\tag{3.33}
$$

where $(1-)$ stands for $(\cos\theta_{k_1} - \sin\theta_{k_1})$, $(2+)$ for $(\cos\theta_{k_2} + \sin\theta_{k_2})$ and so on. A_{12} and A_{21} are two complex numbers to be determined.
Energies can be computed by substituting these ansatzs into the equations obtained projecting on the first four states showed above; the result is a set of four equations, each of which can be split into two parts, multiplying respectively $e^{i(k_1 n_1 + k_2 n_2)}$ and $e^{i(k_1 n_2 + k_2 n_1)}$. A general solution has to be valid for all n_1 and n_2, so the two parts are effectively two distinct (but equivalent) equations. Finally a system of four equations emerges

$$\begin{cases} -J\Big[(1-)(2+)\cos k_2 + (1+)(2-)\cos k_1\Big] - (E-2h)(1-)(2-) = 0 \\ -J\Big[(1-)(2+)\cos k_1 + (1+)(2-)\cos k_2\Big] - (E+2h)(1+)(2+) = 0 \\ -J\Big[(1-)(2-)\cos k_2 + (1+)(2+)\cos k_1\Big] - E(1-)(2+) = 0 \\ -J\Big[(1-)(2-)\cos k_1 + (1+)(2+)\cos k_2\Big] - E(1+)(2-) = 0 \end{cases} \tag{3.34}$$

There are four variables in four equations, so a relation for the energies can be extracted

$$E^4 - 2\Big(2h^2 + J^2(\cos^2 k_1 + \cos^2 k_2)\Big)E^2 + J^4(\cos^2 k_1 - \cos^2 k_2)^2 = 0 \tag{3.35}$$

Let's define $E^2 = \tilde{E}$ so that, after some algebra

$$\begin{aligned} \tilde{E}_{1,2} &= \underbrace{(J^2\cos^2 k_1 + h^2)}_{E_{k_1}^2} + \underbrace{(J^2\cos^2 k_2 + h^2)}_{E_{k_2}^2} + \\ &\pm 2\underbrace{\sqrt{J^2\cos^2 k_1 + h^2}\sqrt{J^2\cos^2 k_2 + h^2}}_{E_{k_1}E_{k_2}} = \\ &= (E_{k_1} \pm E_{k_2})^2 \end{aligned} \tag{3.36}$$

In conclusion, there are four energies for the system in the $M = 2$ sector:

$$E = \begin{cases} -(E_{k_1} \pm E_{k_2}) \\ +(E_{k_1} \pm E_{k_2}) \end{cases} \tag{3.37}$$

There are still two equations to be satisfied and they determine the ratio between A_{12} and A_{21}.
Subtracting the fifth equation from the third and the sixth equation from the fourth (both for $n_2 = n_1$):

$$\begin{cases} f_{DD}(n_1, n_1) + f_{PP}(n_1 + 1, n_1 + 1) = 0 \\ f_{DD}(n_1 + 1, n_1 + 1) + f_{PP}(n_1, n_1) = 0 \end{cases} \tag{3.38}$$

Using the ansatzs 3.33 we finally reach the relation between the coefficients:

$$(A_{12} + A_{21})\underbrace{(1+)(2+)\Big[1 - e^{i2(k_1+k_2)}\Big]}_{\neq 0 \ \textit{in general}} = 0 \quad \Longrightarrow \quad \frac{A_{12}}{A_{21}} = -1 = e^{i\pi} \tag{3.39}$$

We do not proceed any further with the XX model. However, it is easy to see that these results are in perfect agreement with the ones drawn through Jordan-Wigner transformation for $M = \{0, 1, 2\}$. The next step is the study of the XXZ model with the same technique used until now; in that case, the presence of z-spin interactions will complicate the problem, so that a solution cannot be found.

3.3 XXZ + h staggered model: Bethe Ansatz approach

After all the work done before, it is now time to extend the analysis to the XXZ + h staggered model; the anisotropy constant is defined as Δ, so that the hamiltonian has the form

$$H = -J \sum_{i=1}^{N} \left\{ \frac{1}{2} [S_i^+ S_{i+1}^- + S_i^- S_{i+1}^+] + \Delta S_i^z S_{i+1}^z \right\} + h \sum_{i=1}^{N} (-1)^i S_i^z \tag{3.40}$$

The addition of the z-spin interaction term does not change the commutation relation $[H, S_{tot}^z] = 0$, hence the hamiltonian can still be divided into sectors labelled by the number of down spins. However it adds another nearest-neighbour interaction that supports parallel or antiparallel alignment of spins, depending on the sign of Δ.

In the sector $M = 0$ $|\uparrow\uparrow \dots \uparrow\rangle$ and $|\downarrow\downarrow\downarrow \dots \downarrow\rangle$ are still eigenstates, but their eigenvalues change because of the effect of interaction: $E(M = 0) = -\frac{J\Delta N}{4}$.

In $M = 1$ we build an eigenstate as in 3.22, distinguishing between even and odd. Calculations are identical to the ones for the XX model, except for an adding contribution from

$$-J\Delta \sum_{i=1}^{N} S_i^z S_{i+1}^z |\psi\rangle = -\frac{J\Delta}{4}(N-4)|\psi\rangle \tag{3.41}$$

So we compute eq 3.24 and then project on the two different states with the down spin respectively on a odd or a even site. Using the modified Bethe Ansatz of eq. 3.23 we obtain

$$\begin{cases} -\frac{J}{2} A_P \left[1 + e^{-i2k}\right] - A_D \left(E - h + \frac{J\Delta}{4}(N-4)\right) e^{-ik} = 0 \\ -\frac{J}{2} A_D \left[e^{-ik} + e^{ik}\right] - A_P \left(E + h + \frac{J\Delta}{4}(N-4)\right) = 0 \end{cases} \tag{3.42}$$

So the effect of anisotropy on the energy is a simple shift (dependent from Δ). Note that these equations become identical to 3.25 after defining $E' = E + \frac{J\Delta}{4}(N-4)$; therefore, energies are

$$E^{\pm} = -\frac{J\Delta}{4}(N-4) \pm \sqrt{J^2 \cos^2 k + h^2} = E_\Delta \pm E_{XX} \tag{3.43}$$

In the coefficients calculus, we use eq 3.26 with E' instead of E; however $E' = \pm E_{XX}$ so we obtain the same results of the XX model, which are recalled here for clarity:

$$\frac{A_D}{A_P} = \pm \frac{\cos\theta_k \mp \sin\theta_k}{\cos\theta_k \pm \sin\theta_k} \tag{3.44}$$

$$|\psi^-\rangle = \frac{1}{\sqrt{N}} \sum_{j=1}^{N} \left[(\cos\theta_k + (-1)^j \sin\theta_k) e^{ikj} S_j^- \right] | \uparrow\uparrow \dots \uparrow \rangle \tag{3.45}$$

$$|\psi^+\rangle = \frac{1}{\sqrt{N}} \sum_{j=1}^{N} \left[(-\sin\theta_k + (-1)^j \cos\theta_k) e^{ikj} S_j^- \right] | \uparrow\uparrow \dots \uparrow \rangle \tag{3.46}$$

Let's go on analysing the $M = 2$ sector. Evaluating $H|\psi\rangle = E|\psi\rangle$ and then projecting on all the possible states brings equations just slightly different from the XX model ones: the only differences are energy renormalizations (as in $M = 1$). In particular, the first four equations (for energies) can be recovered by substituting $E' = E + \frac{J\Delta}{4}(N-8)$, while the last two (for coefficients) acquire the same form of the XX model ones through a little change $E'' = E + \frac{J\Delta}{4}(N-4)$.
So the energies of the XXZ + h staggered model are found to be

$$E = \begin{cases} -\frac{J\Delta}{4}(N-8) - (E_{k_1} \pm E_{k_2}) \\ \\ -\frac{J\Delta}{4}(N-8) + (E_{k_1} \pm E_{k_2}) \end{cases} \tag{3.47}$$

As for the coefficients calculus, the same passages used before are applied; the result is a set of two equations more complicated than for the XX model

$$\begin{cases} f_{DD}(n_1, n_1) + f_{PP}(n_1+1, n_1+1) - 2\Delta f_{DP}(n_1, n_1+1) = 0 \\ f_{DD}(n_1+2, n_1+2) + f_{PP}(n_1+1, n_1+1) - 2\Delta f_{PD}(n_1+1, n_1+2) = 0 \end{cases} \tag{3.48}$$

Applying the ansatz 3.33 and bringing the calculations further, we however find no solution to this system. The problem is hidden in the modification of the usual Bethe ansatz: in this study, it is necessary to use coefficients depending on the momenta and the sites parity, instead of constants. So, the two equations in 3.48 cannot be led neither to the same equation, nor to a system with a solution.
Probably the initial idea of using the same ansatz on the XX +h staggered and on the XXZ + h staggered models was wrong. The solution should perhaps be found adopting a different ansatz, but it is hard to tell what its form has to be like.
Therefore, no analytical solution is found for the XXZ + h staggered model: it would have been very helpful in the continue of the study, but it is not strictly necessary anyway. For the numerical study, there are some results from the

investigation of the quantum sine-Gordon model through quantum field theory arguments that provide enough information to locate where the lowest-energy solitons and breathers are. These are the topics the next sections will deal with.

Chapter 4

Numerical simulations

Despite no useful information has come from the Bethe ansatz approach for generic Δ, some interesting clues can be taken from previous studies of the quantum sine-Gordon model through quantum field theories. For example, Zamolodchikov and Lukyanov have been deeply studying this system and some papers of theirs provide enough information to carry on this study numerically [16] [17]. In particular, they found that the quantum sine-Gordon model has only three kinds of elementary excitations: the quantum soliton, antisoliton and breather. As a consequence, these objects should correspond to the lowest-energy states in their spin sectors respectively.
The DMRG (Density Matrix Renormalization Group) numerical technique is excellent in order to pinpoint the energies of these excitations, since it is a variational method and gives quite accurate information about the lowest part of the spectrum of a system. It is very suitable to simulate the behaviour of spin chains and it has been broadly employed to achieve all the results in the following: in the first part it is used in its static form to determine the energies of the soliton excitations; in the final part of the work, instead, its time-dependent form is exploited to realize quenches, to observe the out-of-equilibrium behaviour of soliton and breather in different conditions.

The first paragraph gives an overview of some useful results from quantum field theories about the sine-Gordon model.
The second paragraph deals with the DMRG test: in this stage the aim is to find good working conditions (i.e. efficient compromise between maximum number of states in the basis, amount of memory used, etc.); moreover, a study on how to avoid finite-size effects is worked out.
The third paragraph illustrates the main results from static DMRG simulations, such as the soliton energies for different values of the external field and the study of their single-site magnetization along the z-axis.
In the fourth and final paragraph the out-of-equilibrium dynamics of the soliton and the breather after a quench on the hamiltonian parameters is discussed.

4.1 Results from quantum field theories

In the scientific literature there are some works on the quantum sine-Gordon model: it is studied from the quantum field theory point of view, and provide general information about energy spectrum, scaling exponents and correlators in the model. The solutions are quantum fields, abstract objects that it is hard to visualize physically at first glance.
In particular, A. Zamolodchikov has been able to predict theoretically some of this system features, giving information about the solitons in the model [16]. He found that the only elementary excitations in the model are particles associated to the soliton, the antisoliton and the breather (a bound state of the soliton and the antisoliton, as in the classical case). When these particles collide, they should in principle maintain some of their properties after their interaction, in correspondence with their classical counterparts.
These excitations are associated to a particular spin sector, and following the cited works one finds that

- the soliton is in $S^z_{tot} = 1$
- the antisoliton is in $S^z_{tot} = -1$
- the breather is in $S^z_{tot} = 0$

As they are elementary excitations, they should be located in the lowest part of the energy spectrum, with respect to the spin sector they refer to. Thus, DMRG is a very efficient tool for this purpose: it is variational, so very suitable to explore the lowest part of excitation spectra; moreover, it gives the possibility to investigate different spin sectors separately.
Therefore, recalling that in the critical region the ground state is always in $S^z_{tot} = 0$, the breather will be the first excited state in this spin sector; instead, the soliton and the antisoliton will be the lowest-energetic states respectively in $S^z_{tot} = 1$ and $S^z_{tot} = -1$.

S. Lukyanov and A. Zamolodchikov found also how the elementary soliton mass changes as a function of the external parameter in the sine-Gordon potential [17] (the external field magnitude, in the case of the XXZ + h staggered model). Translating their result into our magnetic model, we find

$$M_{sol} \propto h^{\frac{1}{2-K}} \tag{4.1}$$

where K is the Luttinger parameter in eq. 2.40.
This law will be studied in the following sections, to test whether these predictions actually hold in our magnetic model or not. In fact, they are a good way to verify if bosonization holds for the hamiltonian parameters chosen.

4.2 DMRG test

Before starting to simulate a new hamiltonian, it is usually worthwhile to spend some time upon a more well known system, similar to the new one, that could provide useful information about how to perform efficiently the numerical study. In this case, it is convenient to recover some results from the XXZ model *without* staggered external field, so that suitable values for the maximum number of states of the Hilbert space basis and for the amount of memory needed could be found; some options to improve the results, such as symmetries and block reflections, could also be tested.
The main source of approximation in the DMRG algorithm is the finiteness of the number of basis states that can be considered: if only a restricted number of eigenstates plays an important role in the physics of the system, than the approximation will be excellent; on the other hand, if there are too many states relevant, the truncation of some important basis states might bring to more imprecise results and partial symmetry break. The XXZ model is critical in the parameter range $-1 < \Delta < 1$ that interests this study, while the addition of the staggered field makes the model gapped. The former is harder to simulate than the latter, since its eigenvalues spectrum decays in a slower way; hence, to have a faithful outcome, a larger number of basis states is necessary. If we find a good number of states for the gapless model, it would probably work for the gapped model too.

Above all of this, another crucial issue that must be taken into account is the effect of the finiteness of the system. In fact, all the results from quantum field theories are extracted in the thermodynamic limit (i.e. infinite number of sites in the chain), so that the system behaviour is not affected by edge sites and boundary conditions. It is important to sufficiently avoid finite-size effects in order to compare the numerical outcomes to the analytical ones.
Moreover, the choice of the boundary condition for the hamiltonian deeply influences what can be seen from the simulation: only the right one will show the soliton solutions we are looking for in real space.

4.2.1 Test on the XXZ model

The XXZ model with periodic boundary conditions and in its critical region is known to be described by a $c = 1$ conformal field theory (CFT), where c is the so-called central charge and characterizes the universality class of the model. From these theories, some relations between the energies and the size of the system are exactly calculated; the aim of this section is to confirm these predictions.

The first relation from CFT arguments involves the entropy and the size of the system

$$S(N) \approx \frac{c}{3} log_2 N \tag{4.2}$$

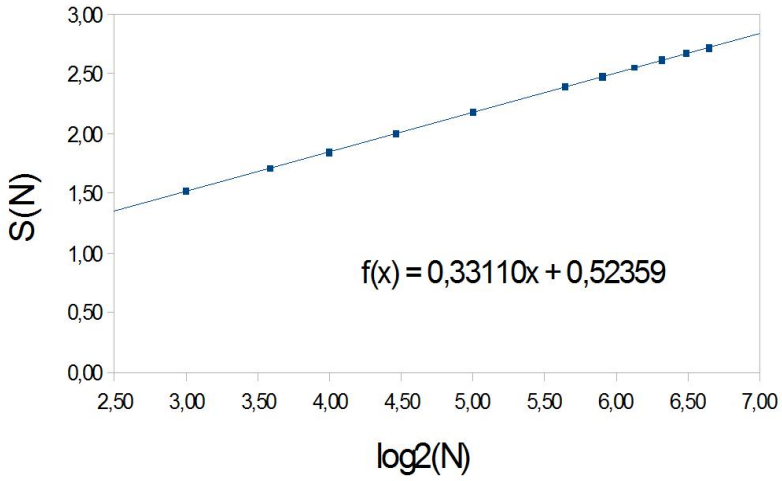

(a) $J = 1;\ \Delta = 0.5$

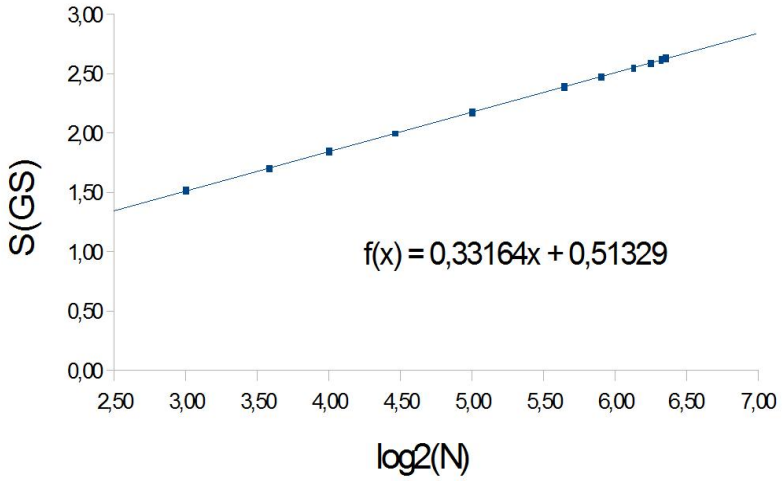

(b) $J = 1;\ \Delta = -0.5$

Figure 4.1: Plot of the entropy as a function of the size of the system for a) the ferromagnetic phase ($J\Delta > 0$) and b) the antiferromagnetic phase ($J\Delta < 0$).

Simulations for chain length N ranging from 8 to 100 have been performed, choosing to evaluate the first five excited states. The outcomes are plotted in Fig. 4.1 for $J = 1$ and the two anisotropy values $\Delta = \pm 0.5$. The linear fit of the outcomes gives quite exactly $c = 1$, confirming that the system simulated is like the one described by the CFT.

Then, another relation from CFT quantifies how much the ground state energy at finite size differs from the ground state energy in the thermodynamic limit

$$e_{GS}(N) - e_{GS}^{LT} = -\frac{\pi}{6}\frac{cu}{N^2} \tag{4.3}$$

where "LT" stands for "Thermodynamic limit", the e functions are single-site energies ($\frac{E(N)}{N}$) and u is the so-called effective velocity, the parameter that can be found in the quantum sine-Gordon model in eq. 2.44 and that is concerned with the kinetic energy.
Recalling the results explained in the second chapter, eq. 2.41 provides theoretical values for the effective velocities from exact Bethe ansatz calculations. Our numerical simulations are in great agreement with them, as can be seen in Fig. 4.2; in both the cases under study, setting $c = 1$ the effective velocity coincides within some units of 10^{-2}

$J\Delta$	Numerical	Analytical	Difference
0.5	0,656	0,649	7 x 10^{-3}
-0.5	1,328	1,299	2.9 x 10^{-2}

The last equation taken from CFT involves the so-called *scaling dimensions*: they are labelled as d_{nm}, where m is linked to a conserved quantity (the total z-spin in our magnetic model) and n is a positive integer number. The scaling dimensions permit to divide the Hilbert space into sectors and to classify the excited states within each of them; this is clearer looking at the form these quantities are usually written in

$$d_{nm} = n^2 K + \frac{m^2}{4K} + j + j' \tag{4.4}$$

where K is the Luttinger parameter expressed in eq. 2.40, j and j' are positive integer numbers.
When $j = j' = 0$, the scaling dimension refers to the lowest-energetic state within the nm sector. Then, successive excitations can be built by simply adding positive integer values.
These quantities influence the gap between the ground state energies and their respective excited state energies. In fact, the following relation holds

$$E_n - E_{GS} = \frac{2\pi}{N} d_{nm} v \tag{4.5}$$

Scaling dimensions have been computed for $J = 1$, $\Delta = \pm 0.5$ for the first four excited states in the sectors $S^z_{tot} = m = 0, 1, 2$. These results have been

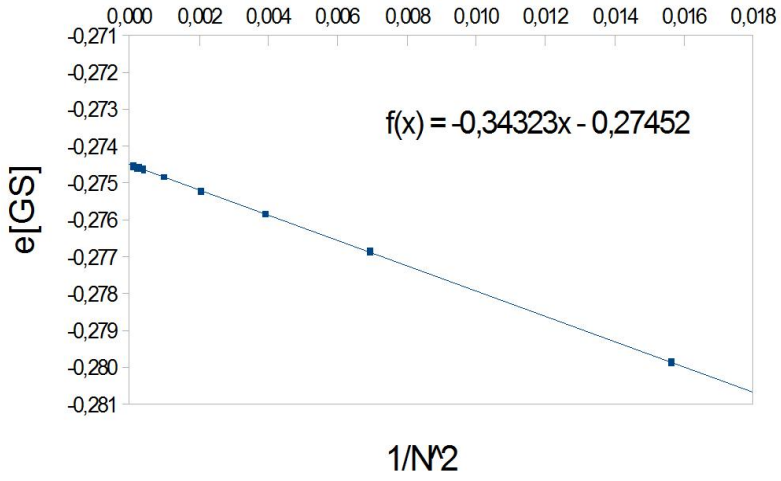

(a) $J = 1;\ \Delta = 0.5$

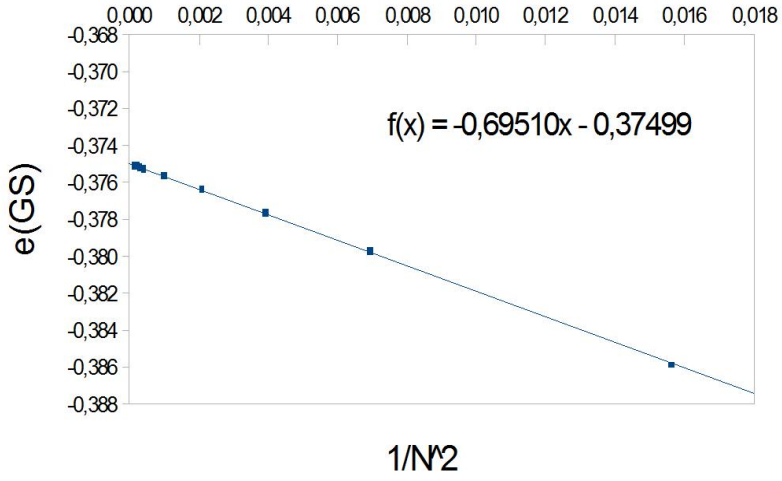

(b) $J = 1;\ \Delta = -0.5$

Figure 4.2: Plot of the single-site ground state energy as a function of the size of the system for a) the ferromagnetic phase ($J\Delta > 0$) and b) the antiferromagnetic phase ($J\Delta < 0$).

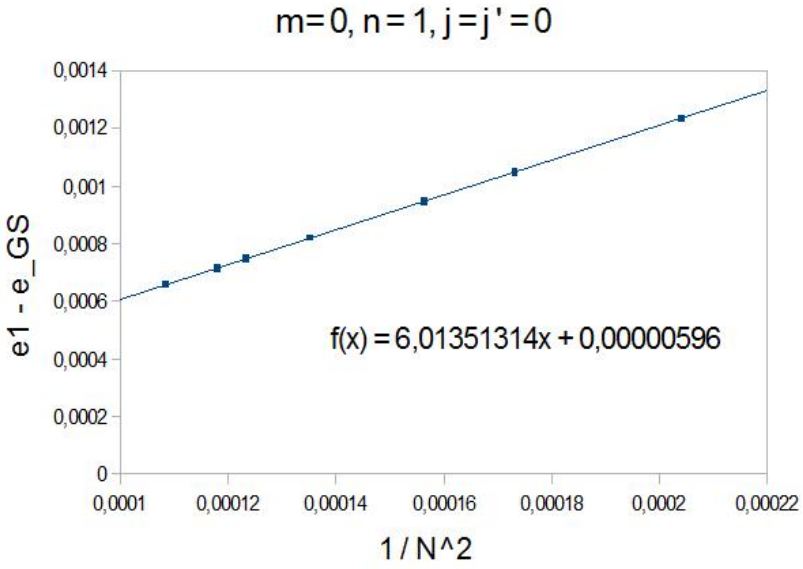

$\Delta = -0.5$, ground state for m = 0, n = 1

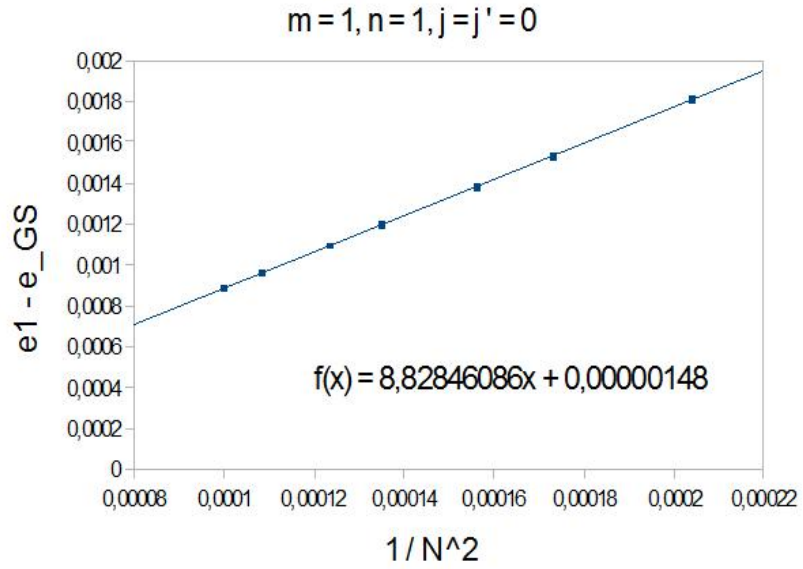

$\Delta = -0.5$, ground state for m = 1, n = 1

Figure 4.3: Plots of the excitation gaps vs squared reciprocal of the size, used to calculate some of the results shown in tables 4.1 and 4.2.

obtained from linear fits of the data, as illustrated for some cases in Fig.s 4.3.

All the outcomes are summarized in tables 4.1 and 4.2, next to their respective theoretical values and the differences between them. They all agree with the expected figures within 10^{-2}: it is a proof of quite accurate simulations. Probably, the error comes in part from finite-size effects, since the thermody-

$S_z = m$	classification (n-j-j')	Analytical	Numerical	Difference
0	1 - 0 - 0	0,75	0,73678	-0,01322
0	-1 - 0 - 0	0,75	0,76156	0,01156
0	0 - 1 - 0	1	0,99879	-0,00121
0	0 - 0 - 1	1	0,99792	-0,00208
1	0 - 0 - 0	0,33333	0,33330	-0,00003
1	-1 - 0 - 0	1,08333	1,08169	-0,00164
1	-1 - 0 - 0	1,08333	1,08167	-0,00166
1	0 - 1 - 0	1,33333	1,32946	-0,00387
1	0 - 0 - 1	1,33333	1,32850	-0,00483
2	0 - 0 - 0	1,33333	1,33021	-0,00312
2	1 - 0 - 0	2,08333	2,07603	-0,00729
2	-1 - 0 - 0	2,08333	2,07603	-0,00731
2	0 - 1 - 0	2,33333	2,31850	-0,01483
2	0 - 0 - 1	2,33333	2,31776	-0,01557

Table 4.1: Scaling dimensions for $J = 1$ and $\Delta = -0.5$.

$S_z = m$	classification (n-j-j')	Analytical	Numerical	Difference
0	0 - 1 - 0	1	1,00187	0,00187
0	0 - 0 - 1	1	1,00119	0,00119
0	1 - 0 - 0	1,5	1,49984	-0,00016
0	-1 - 0 - 0	1,5	1,49984	-0,00016
1	0 - 0 - 0	0,16667	0,16668	0,00001
1	0 - 1 - 0	1,16667	1,16554	-0,00112
1	0 - 0 - 1	1,16667	1,16583	-0,00084
1	1 - 0 - 0	1,66667	1,66325	-0,00342
1	-1 - 0 - 0	1,66667	1,66218	-0,00448
2	0 - 0 - 0	0,66667	0,66534	-0,00132
2	0 - 1 - 0	1,66667	1,66031	-0,00635
2	0 - 0 - 1	1,66667	1,66045	-0,00621
2	1 - 0 - 0	2,16667	2,15503	-0,01163
2	-1 - 0 - 0	2,16667	2,15495	-0,01171

Table 4.2: Scaling dimensions for $J = 1$ and $\Delta = 0.5$.

namic limit may never be reached. These first simulations helped in finding good working conditions: 400 maximum states for the Hilbert space basis, a number of sites between 70 and 100 and an amount of memory of some Giga-Bytes provide accurate simulations in a reasonable lapse of time (a few hours). After having set these basic DMRG parameters, the study of the XXZ + h staggered model was started.

4.2.2 Study of finite-size effects

Another issue that must be faced before starting the soliton research concerns how the finiteness of the chain influences the results. As we are based on theoretical results taken at the thermodynamic limit, it is important to mimic the same regime in the numerical simulations too. However, for different values of the parameters in the hamiltonian, finite-size effects may change from negligible to relevant: the aim of this section is to show how to distinguish these different situations and to explain the final choice of parameters for the simulations done in the following.
For gapped models, it is known that the excitation energies $e(N)$ depend on the number of sites N: they grow up for increasing N, but finally stabilize close to their thermodynamic limit values. What causes this dependence is of course the finiteness of the system. However, if we get very close to the thermodynamic limit value (when N exceeds some units of the so-called correlation length), we can think that finite-size effects are negligible and the behaviour of the system is very similar to an infinite one.
Therefore, simulations have been worked out on the XXZ + h staggered model to pinpoint the soliton masses for different sizes, fixing field and anisotropy values.
Firstly, $J = 1$ and $\Delta = 0.3$ were fixed; this corresponds to the ferromagnetic region. The single-site energy vs the reciprocal of the system size was plotted for different field magnitudes, namely $h = \{0.005,\ 0.01,\ 0.1\}$ (see Fig.s 4.4 and 4.5). For the first two field values no stabilization around an asymptotic figure is observed; hence, finite-size effects would not be negligible in these regimes. Instead, for $h = 0.1$ the trend is found to stabilize starting from around $N = 50$, as can be seen in Fig. 4.5. Thus, this field value is suitable for future simulations when $J = 1$, $\Delta = 0.3$ and $N \geq 50$ are taken.
Let's see now if the same holds for the other phase region in $J = 1$ and $\Delta = -0.3$. Simulations have been worked out for $h = 0.1$ and the result is shown in Fig. 4.6. For these parameter values also finite-size effects are negligible, and the limitation on the size seems also less stringent then before ($N \geq 30$).
Therefore, the following parameters have been chosen to correctly look for solitons in the model

$$\begin{array}{ll} J = 1 & \Delta = \pm 0.3 \\ N = 70 & h = 0.1 \end{array}$$

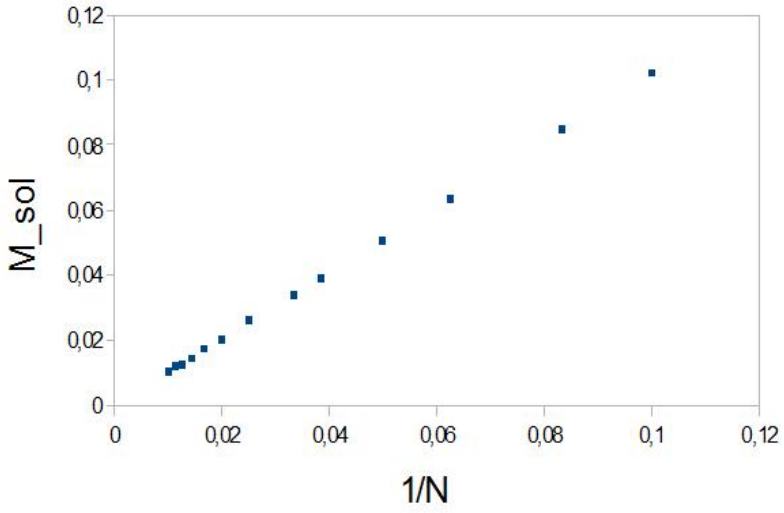

(a) $h = 0.005$

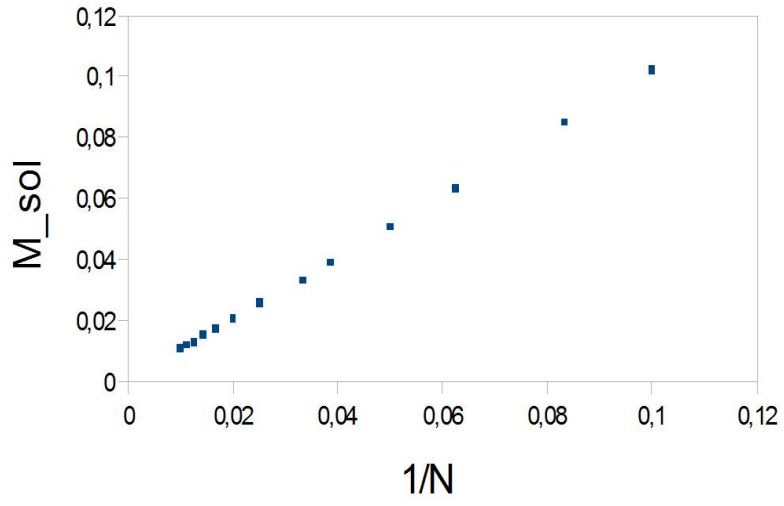

(b) $h = 0.01$

Figure 4.4: Plot of the soliton mass as a function of the size of the system for $J = 1$, $\Delta = 0.3$ and a) $h = 0.005$ and b) $h = 0.01$. These field values are too low to avoid finite-size effects, as no stabilization is seen for the highest investigated values of N.

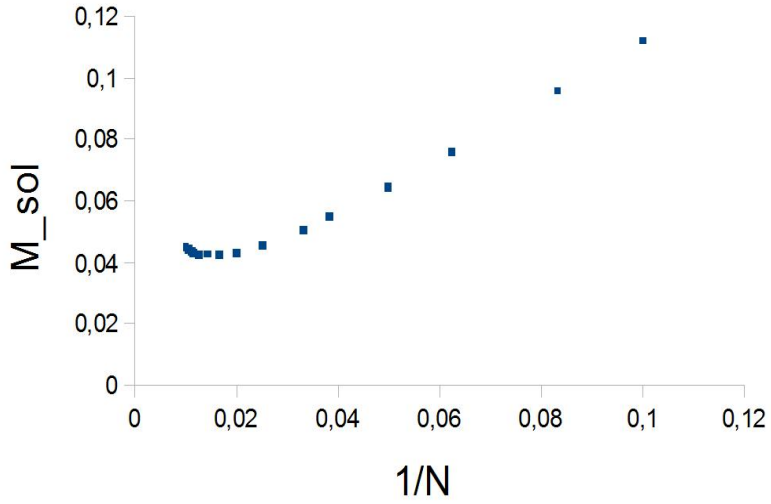

Figure 4.5: Plot of the soliton mass as a function of the reciprocal of the size for $h = 0.1$: a clear stabilization is found. Note that the trend is not monotonic, but after the minimum the thermodynamic limit energy is expected to increase very slightly.

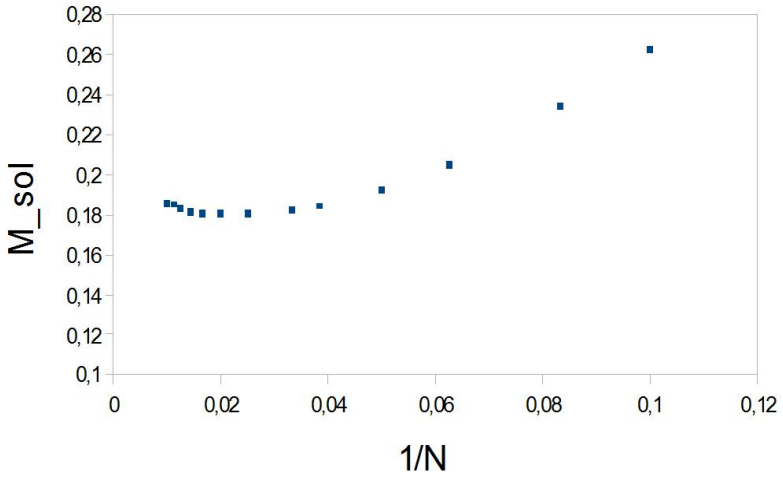

Figure 4.6: For $J = 1$ and $\Delta = -0.3$ the trend is the same as in Fig. 4.5; here stabilization begins even for smaller size values.

4.3 Static DMRG simulations

Having found a set of parameter values so that finite-size effects are negligible, we can carry out static simulations to locate the soliton energies and their dependence on the magnitude of the staggered field; the outcomes would then be comparable to the thermodynamic limit ones.
Static simulation means that, given the hamiltonian, eigenvalues and observables on the eigenstates are computed. Hence, the system is studied on the equilibrium. This is different from what will be shown in the next section, when the out-of-equilibrium behaviour of the system will be investigated.

4.3.1 Scaling exponents for the soliton mass

As stated before, arguments from CPT give a precise exponential relation between the soliton mass and the magnitude of the field. For a low enough value of h, the scaling exponent depends uniquely on the Luttinger parameter K, which in turn depends uniquely on the anisotropy Δ.
If we put eq. 2.40 into eq. 4.1, we obtain the trend of the soliton mass as a function of Δ

$$M_{sol} \propto h^{\frac{1}{2-K}} = h^{\frac{2\arccos(\Delta)}{4\arccos(\Delta)-\pi}} \tag{4.6}$$

For $\Delta \approx 0.7$ there is a singularity and the scaling exponent behaviour around this value is hard to predict. We will stay away from that point, exploring regions with $\Delta = \pm 0.3$. The reason for this choice is, beside the motivation just shown, that for anisotropy values in module greater than 0.5 the theory predicts the existence of more than one breather in the lowest part of the excitation spectrum. Thus, to avoid complications, it is convenient to sit in regions where there is only one bound state to characterize.

In this part of the work, it is proved that the predicted scaling exponents are in very good agreement with DMRG numerical simulations for our previous choice of parameters in the hamiltonian. This means that arguments from CPT on the quantum sine-Gordon model hold for this magnetic model too (at least for the parameters considered here). This confirmation is important because we will highly ground on these theoretical predictions in the following.
Simulations to compute the mass of the lowest-energetic soliton as a function of the external field have been carried out. Quantum field theories applied to the quantum sine-Gordon model tell that the soliton is the first excitation in the spin sector $S_z = 1$; so, its mass is calculated as the difference between the lowest-energy state in $S_z = 1$ and the ground state energy (in $S_z = 0$).
In order to avoid finite-size effects, only field values greater than or equal to 0.1 have been considered; of course, they have also to be low enough to be felt as a perturbation on the system. Hence, field values in the range $[0.1, 0.3]$ have been chosen.
For $\Delta = \pm 0.3$, the relation between the soliton mass and the magnitude of the

field is plotted in Fig 4.7. Non-linear fits have been realized through the GNUplot software: the results are in good agreement with the theory, showing a scaling exponent minor (greater) than one in the antiferromagnetic (ferromagnetic) region. The results are shown in table 4.3: they are in good agreement with the ones predicted by the theory. Hence, we can consider the theoretical analysis of the sine-Gordon model done by means of quantum field theory trustworthy. Basing on them, we can now start the study of the excitation masses.

Δ	Theoretical	Numerical	Difference
-0,3	0,86024	0,82943	0,03081
0,3	1,31692	1,19279	0,12413

Table 4.3: Results for scaling exponents.

4.3.2 Soliton excitation energies and properties

In this part, the masses of the lowest-energetic soliton, antisoliton and breather are computed for the choice of parameters specified before. These energy gaps are calculated with respect to the ground state energy, that is always in the $S_z = 0$ spin sector. Then, the lowest-energetic breather is the first excitation in the same sector. Instead, the lowest-energetic soliton and antisoliton are the lowest-energetic states respectively in $S_z = 1$ and $S_z = -1$; they are expected to have the same mass, and to be put one into the other through an inversion transformation of both the z-spins and the external field directions.
Moreover, the breather is expected to sit only in one of the two subregions of the critical phase of the model.

Chains with $N = 70$ sites have been studied with $J = 1$, $\Delta = \pm 0.3$ and external field values in the range $h = [0.05, 0.2]$. The DMRG technique is able to divide the hamiltonian eigenvalue spectrum into sectors defined by a conserved additive quantum number (such as the total z-spin): this is very useful to search into separate sectors and discriminate between the soliton, the antisoliton and the breather.
All the masses found are listed in tables 4.4 and 4.5. In particular, the existence of the breather can be evaluated by checking whether its energy is lower than twice the soliton mass. In fact, since the breather is a sort of bound state of a soliton and an antisoliton, it will have to lower the total energy of its components.
This estimation is given in Fig.s 4.8 and 4.9 for the two anisotropy values considered. As expected, it is found that only one of the two points exhibits a breather excitation, namely the one corresponding to the antiferromagnetic region. In the other one, the supposed breather has energy higher than twice the soliton mass, so it cannot be the expected bound state; it simply is another

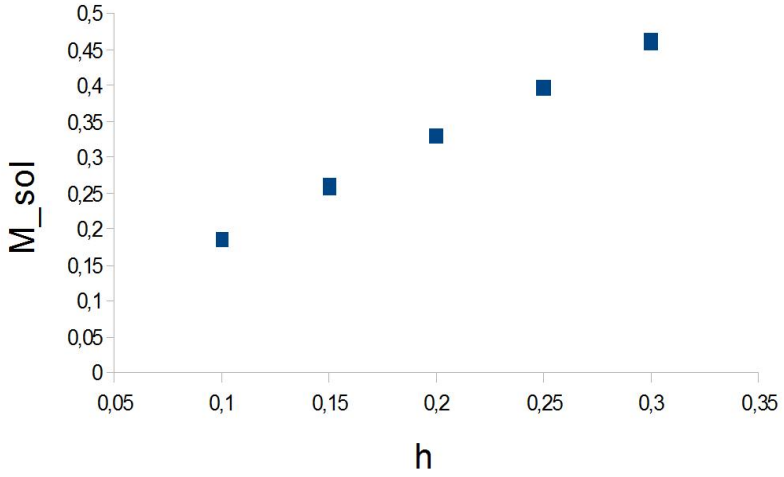

(a) $\Delta = -0.3$

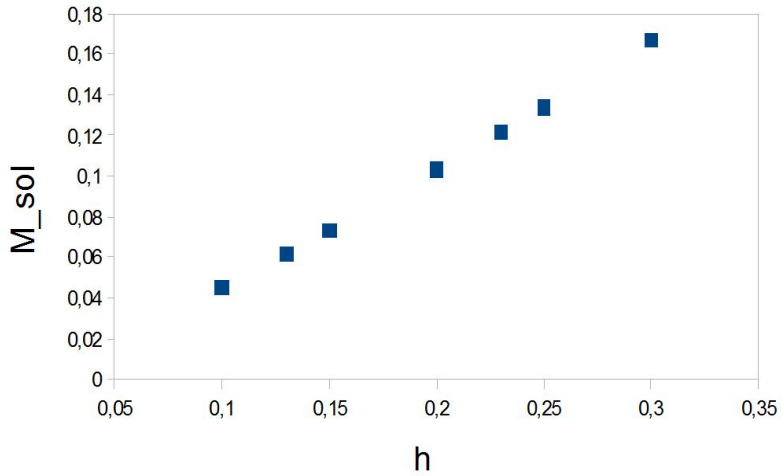

(b) $\Delta = 0.3$

Figure 4.7: Trend of the soliton mass as a function of the external field magnitude for points in a) the antiferromagnetic region and b) the ferromagnetic region. Non-linear fitting proves that this behaviour differs slightly from the linear one, with exponents for the field expressed in table 4.3.

h	(Supposed) Breather mass	Soliton mass	2 x soliton mass
0,05	0,0865895796	0,0237018598	0,0474037197
0,08	0,1027779887	0,0341455737	0,0682911474
0,1	0,1165264102	0,0434362661	0,0868725322
0,15	0,161532279	0,070656957	0,141313914
0,2	0,2156242996	0,0990512847	0,1981025694

Table 4.4: Lowest-energetic soliton excitation masses for different field magnitudes at $\Delta = 0.3$.

h	Breather mass	Soliton mass	2 x soliton mass
0,05	0,1937240109	0,1016224222	0,2032448443
0,08	0,2773075485	0,1507700998	0,3015401995
0,1	0,3326459197	0,1807372401	0,3614744802
0,15	0,4676354734	0,2563462611	0,5126925222
0,2	0,5961000915	0,326191106	0,652382212

Table 4.5: Lowest-energetic soliton excitation masses for different field magnitudes at $\Delta = -0.3$.

kind of excited state not interesting for this thesis purposes.
In Fig. 4.9, however, the breather mass is only slightly lower than the sum of its components masses, so that one could object that there could be uncertainty due to errors. As for numerical errors, DMRG provides a truncation error, calculated as the sum of all the eigenvalues thrown away during the approximation process; it is usually of the order of 10^{-8}. Then, it is hard to predict an error on the energies, but it is usually considered that this error is proportional to the truncation one. Since, the truncation error is very much lower than the difference between the masses under consideration, we can retain that the numerical error is negligible.
On the other hand, however, finite-size effects affect the calculation when the field is too low. Probably, this is why the two calculated masses are very close together for $h = 0.05$. Nonetheless, if we take a high enough field magnitude (such as $h = 0.1$), there are no problems in identifying the breather existence.
These results give a very interesting possibility to realize an entangled state of a soliton and an antisoliton: one can prepare a stable breather in the antiferromagnetic region and then realize a quench to shift into the ferromagnetic one. In the latter region, the breather is no more an eigenstate and then should split into a soliton-antisoliton pair. They would probably be entangled and this system might be a suitable candidate for a two-qubit state realization.

In this case, however, it is necessary to check whether the breather mass in the antiferromagnetic region is greater than twice the soliton mass in the ferromagnetic region. This is important because, after the quench, we would like the soliton and the antisoliton to have non-zero kinetic energy, so that

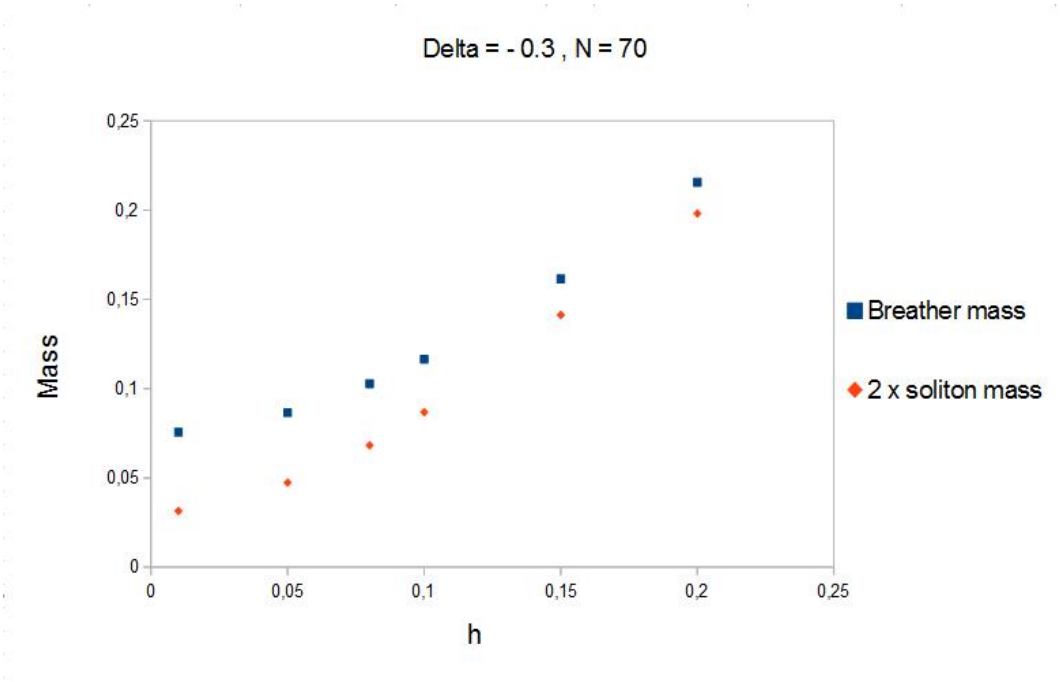

Figure 4.8: Supposed breather mass vs twice the soliton mass for $J = 1$ and $\Delta = 0.3$ (ferromagnetic region). In this case the breather is not present, as its mass should be higher than the sum of its components masses.

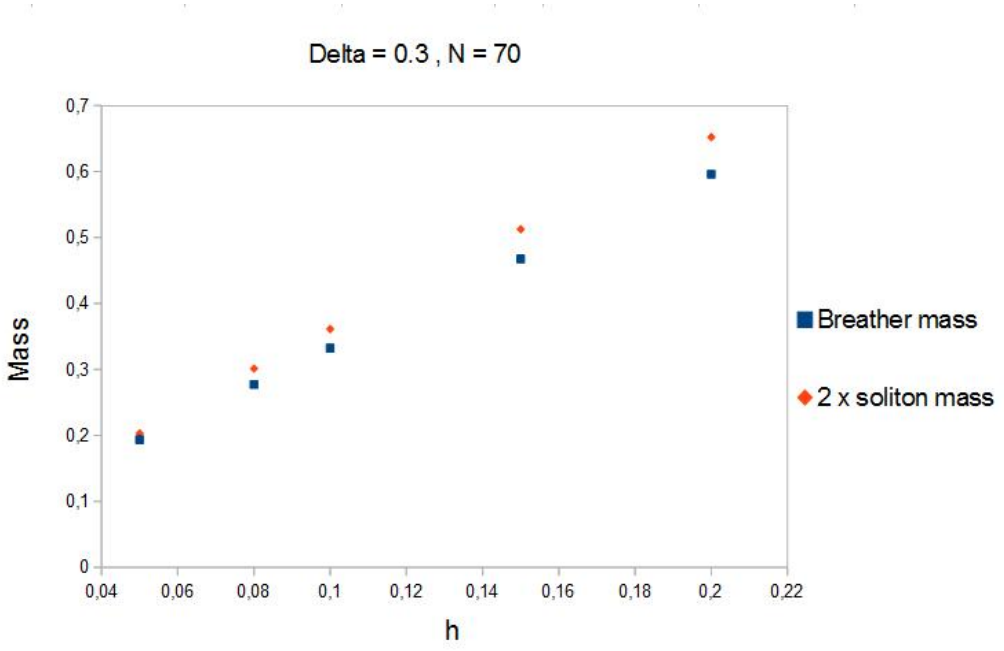

Figure 4.9: Breather mass vs twice the soliton mass for $\Delta = -0.3$. Here the breather exists for all the field values examined, at least higher than 0.05.

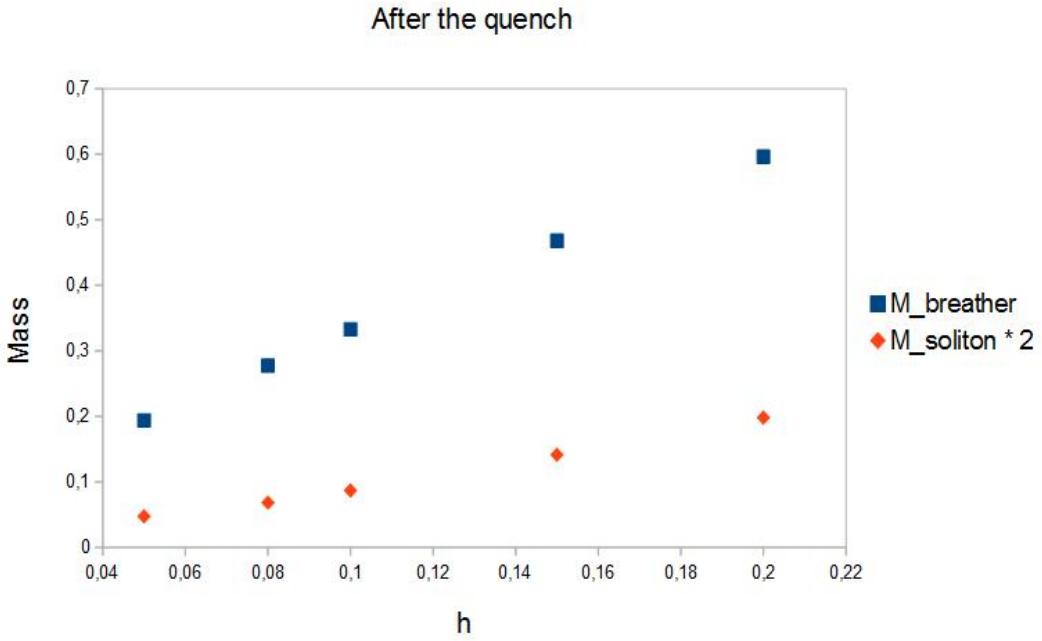

Figure 4.10: Breather mass in the AFM region vs twice the soliton mass in the FM region. .

they could move along the chain.
This condition widely holds for all the field values considered, as can be seen in Fig. 4.10. Note that it is a necessary but not sufficient condition, since before and after the quench the total system energy changes. These results however keep the door open to this opportunity, to be exploited after the breather and soliton spatial behaviours will be understood better.

Before investigating the time-evolution of the system after a quench, it is fundamental to determine how to monitor and characterize the soliton and the breather through observables.
One and two-point operators are usually employed for this purpose. In this case, they are the single-site magnetization along the z-axis ($\hat{S}^z_j$) and the correlators for the magnetization along the z-axis ($\hat{S}^z_j \hat{S}^z_k$) and for the x-y plane ($\hat{S}^+_j \hat{S}^-_k$).
When translational invariance is present, the application of one-point operators on each site gives a flat response: in fact, a measure on one site must yield the same result as a measure taken after translating of an arbitrary multiple of twice the lattice constant.
As a consequence, the use of periodic boundary conditions on the chain gives no direct information about the behaviour in space of soliton excitations. A

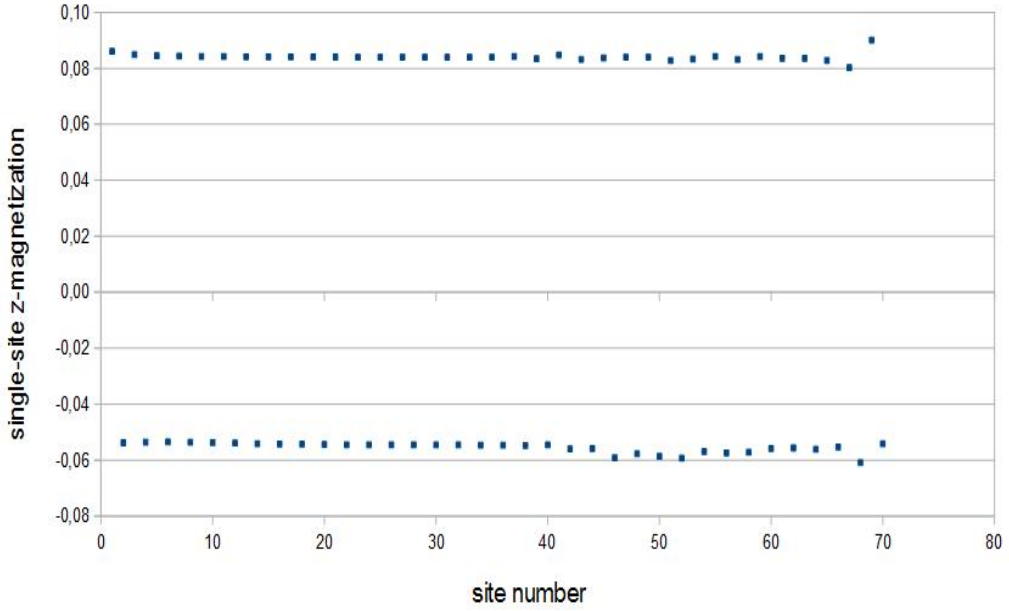

Figure 4.11: Single-site z-magnetization on each site for the soliton with periodic boundary conditions. The two curves are almost flat because of translational invariance of two lattice constants.

plot of the single-site z-magnetization for the soliton is shown in Fig. 4.11: as expected, the trend is nearly flat. Moreover, the presence of the two "bands" derives from the fact that there is translational invariance of two lattice constants (and not only one).

Two-point correlators with periodic boundary conditions may still bring information, but it is convenient to change the point of view and employ *open boundary conditions*. This choice involves no translational symmetry and highlights in some way the structure of the soliton excitations in space.
The soliton properties have been studied for $\Delta = 0.3$ (since it is the value after the quench, when the soliton and the antisoliton should propagate). The single-site z-magnetization behaves as plotted in Fig. 4.12 for $N = 70$ sites. It can be immediately seen that the two "bands" are different in shape; however, it is not straightforward how to extrapolate information from them.
In order to do this, recall eq. 2.32 derived while dealing with bosonization of the magnetic model into the sine-Gordon one. The single-site magnetization has two components: one uniform and slowly varying, the other staggered, i.e. rapidly oscillating.
In particular, from eq. 2.36 the uniform component is proportional to the spatial derivative of the field solution, so it is expected to bring information about the soliton shape. In fact, the latter is classically a bump on a flat background, and if the quantum soliton is linked to the classical one, it is interesting to ob-

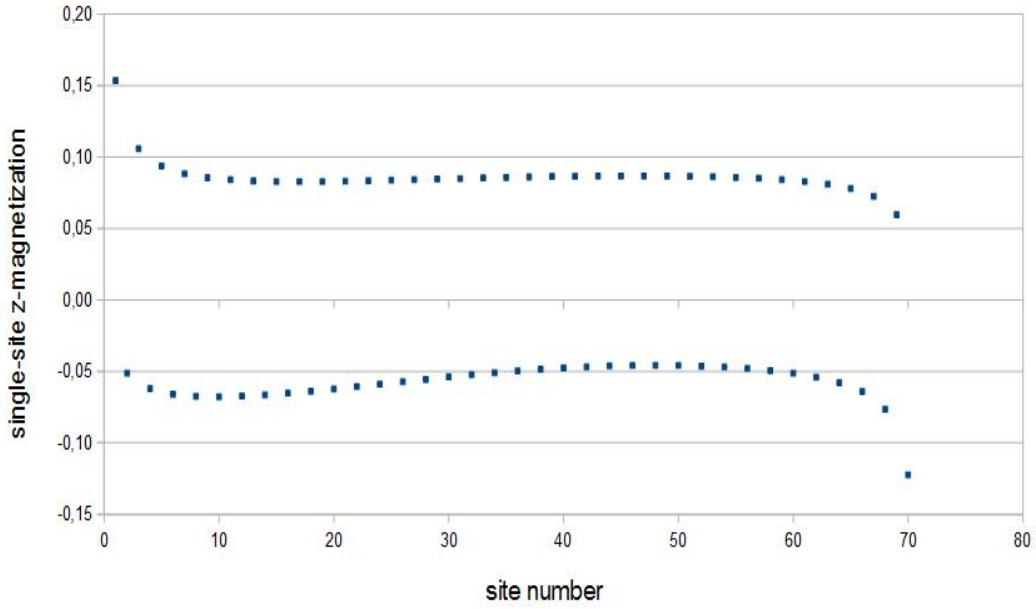

Figure 4.12: Single-site z-magnetization on each site for the soliton with open boundary conditions for $\Delta = 0.3$ and $h = 0.1$. In this case, the two plots are not trivial and contain some interesting physical information.

serve whether this feature already holds or not.
The staggered component is also interesting: from eq. 2.37 it is proportional to the function $\sin(\beta\phi)$, so it depends from the field solution too.
These two components are computed through a simple trick: the z-magnetization on the j-th site and on its nearest-neighbour can be written

$$\begin{aligned} S^z_j &\approx \rho(x) + (-1)^{\frac{x}{a}} M(x) \\ S^z_{j+1} &\approx \rho(x+dx) - (-1)^{\frac{x}{a}} M(x+dx) \approx \rho(x) - (-1)^{\frac{x}{a}} M(x) \end{aligned} \tag{4.7}$$

where, in the last equation, we have expanded in series and then truncated both $\rho(x)$ and $M(x)$, supposing they are smooth functions.
Expressions for the uniform and the staggered components can be easily calculated by inverting eq. 4.7. One finally obtains

$$\begin{aligned} \rho(x) &\approx \frac{S^z_j + S^z_{j+1}}{2} \\ M(x) &\approx (-1)^j \frac{S^z_j - S^z_{j+1}}{2} \end{aligned} \tag{4.8}$$

These two components are plotted in Fig. 4.13 for the soliton with $\Delta = 0.3$ and $h = 0.1$. The uniform part is a sort of bump, but it is all the chain broad; its shape is peculiar and has an orientation towards the right.

It is interesting to see how the bump modifies as the hamiltonian parameters are changed. Simulations have been carried out for the opposite field value $h = -0.1$ and for a longer chain ($N = 120$); the outcomes are respectively shown in Fig.s 4.14 and 4.15. As for the former case, the bump seems the one in Fig. 4.13a after a reflection along an axis orthogonal to the chain. This is due to the staggered field, that gives a preferred orientation on the right or the left, depending on the field direction on even and odd sites. Instead, as for the longer chain case, the bump is seen to reduce in height and broaden to the whole spatial length.
Since the bump changes orientation depending on the sign of the external field, the $h = 0$ has been studied also (Fig. 4.16) to see a sort of transition point from the two different situations. As expected, the plot is symmetric.
However it seems that, for a very high external field value, the bump should be squashed to one edge of the chain. The result of the simulation for $h = 10$ is plotted in Fig. 4.17 and rejects this expected behaviour: it suggests that the physics behind this phenomenon is less intuitive than it may seem at a first glance.
Simulations for the antisoliton have been also realized: they all confirm that it behaves exactly as the soliton with z-spin and field directions inverted, as can be seen from the uniform magnetization plot in Fig. 4.18.

Instead, a different behaviour belongs to the breather. This state shows a peculiar pattern for the uniform magnetization: there are two different and separated curves in the plot, one corresponding to j odd and the other to j even, if we consider eq. 4.8.
This state has been studied for $h = 0.1$ and $h = 0.2$ to see how the shapes modify. The outcomes are illustrated in Fig. 4.19: as a result, increasing the field magnitude yields more linearized curves, but this is hard to interpret. Simulations with much more basis states have been also carried out, to check whether numerical error might have affected the outcomes; z-magnetization plots are exactly the same as before, assuring their numerical correctness.
However, in deriving eq.s 4.8, it was assumed that $\rho(x)$ and $M(x)$ were smooth functions. As can be seen from the plots, this hypothesis is valid for the soliton, but it is not straightforward that it holds for the breather too. In this case, in fact, they do not vary so slowly as for the soliton.
In any case, the plot in Fig. 4.19 shows interesting features and may have a physical meaning. The two curves seem to mimic one soliton and one antisoliton bump partially overlapping. However, these are only qualitative considerations, and only further studies will bring better understanding of these results.
To shed more light on these problems, the soliton and breather time-evolutions have been monitored after quenches on the hamiltonian parameters. As we will see, this takes all the final part of this work.

Uniform component

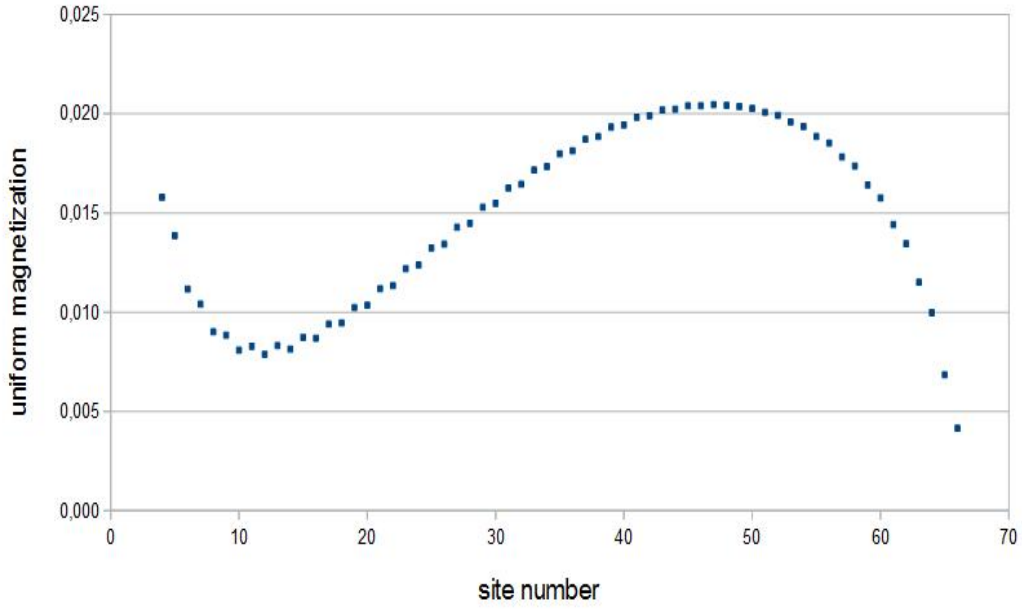

Staggered component

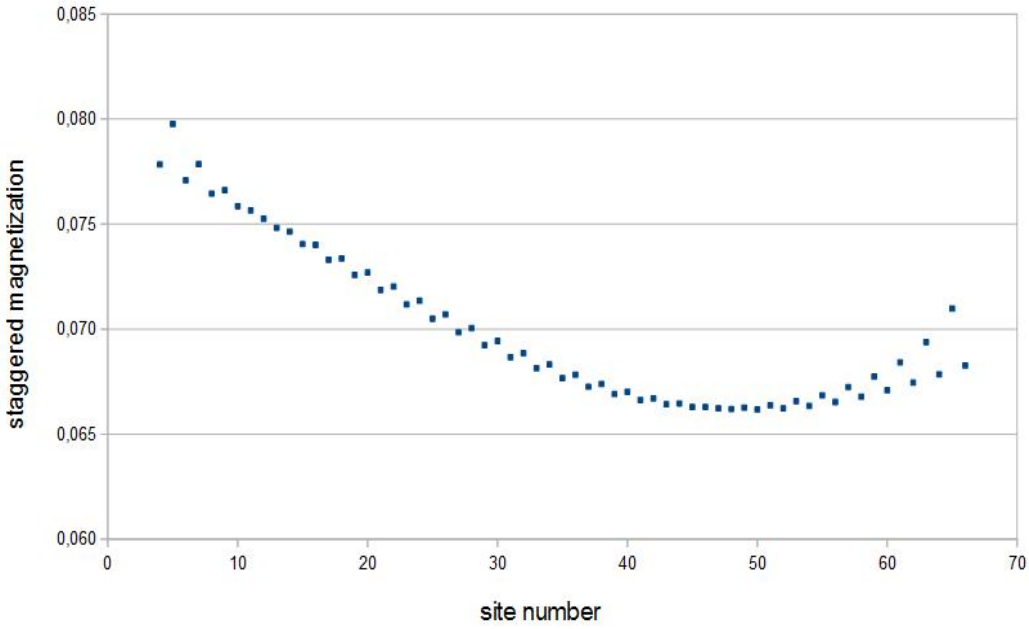

Figure 4.13: Uniform (a) and staggered (b) components of the single-site z-magnetization of the soliton represented in Fig. 4.12.

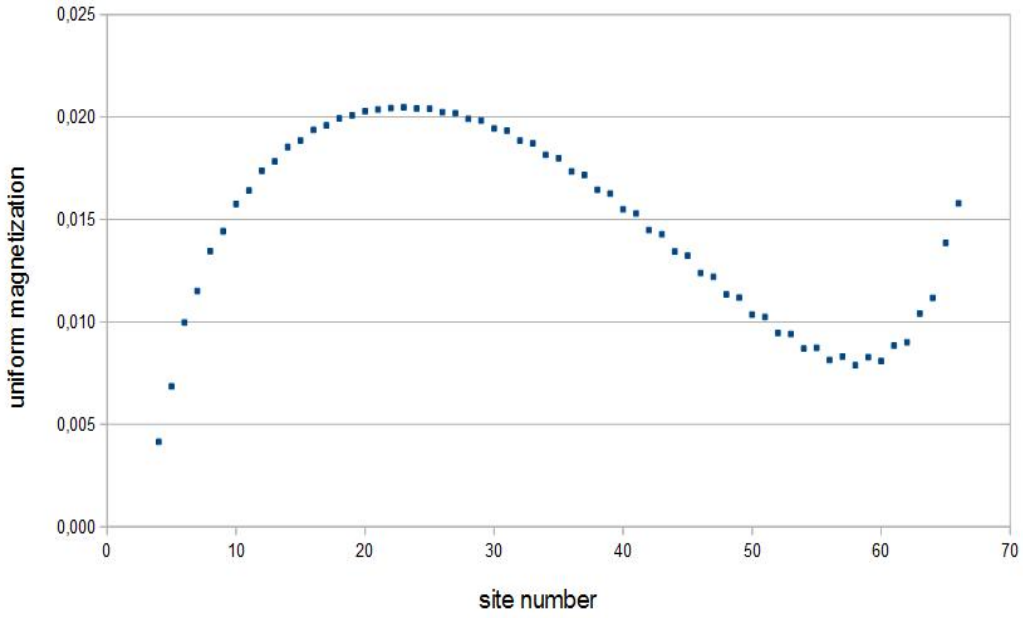

Figure 4.14: Uniform magnetization for an external field with opposite direction than in Fig. 4.13a ($h = -0.1$).

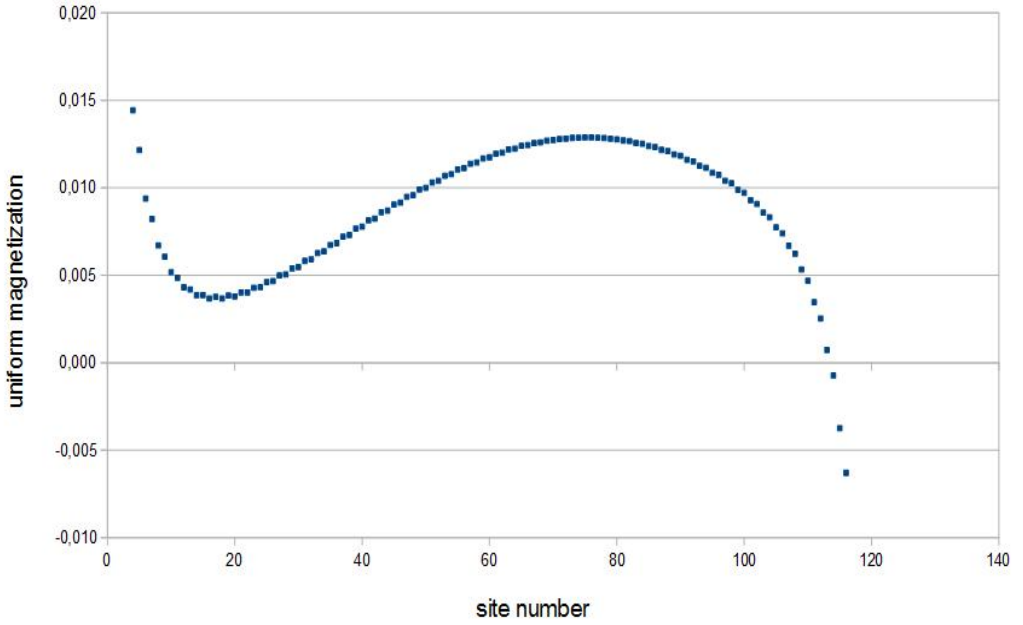

Figure 4.15: Uniform magnetization for a much longer chain ($N = 120$).

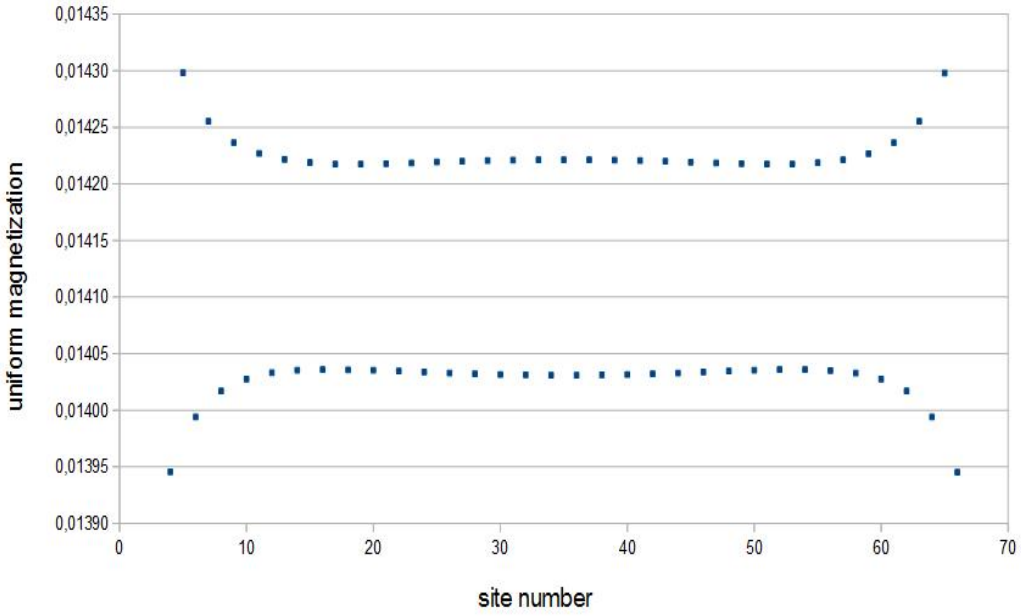

Figure 4.16: Uniform magnetization for the soliton in absence of external field. As expected, the plot is symmetric.

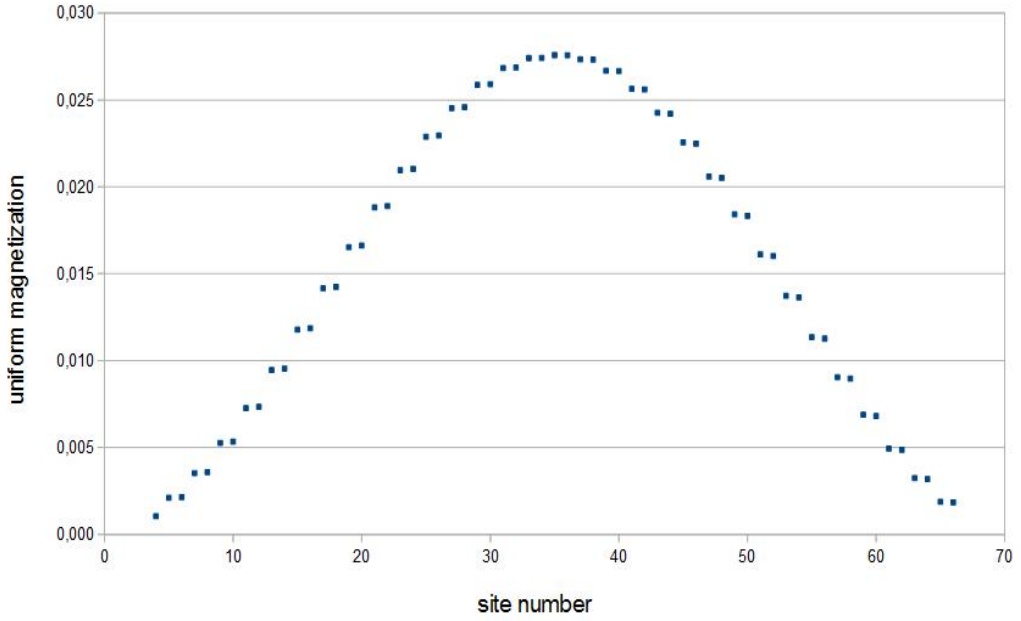

Figure 4.17: Uniform magnetization for the soliton for a very high field magnitude. On the contrary to what expected, the bump becomes nearly symmetric.

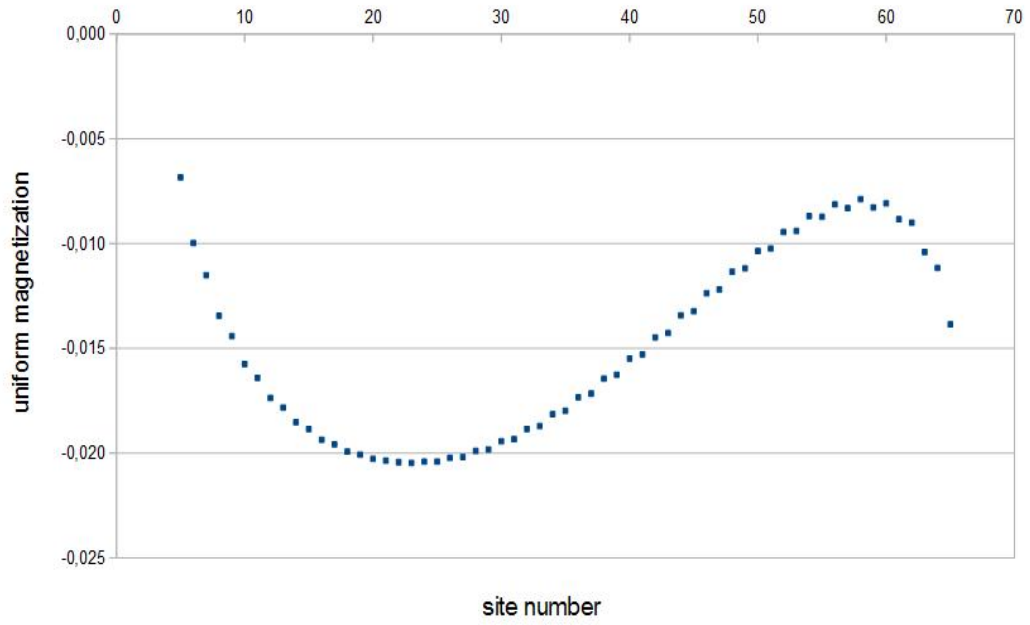

Figure 4.18: Uniform magnetization for the antisoliton with $h = 0.1$. The shape is the same as the soliton one after symmetry transformation.

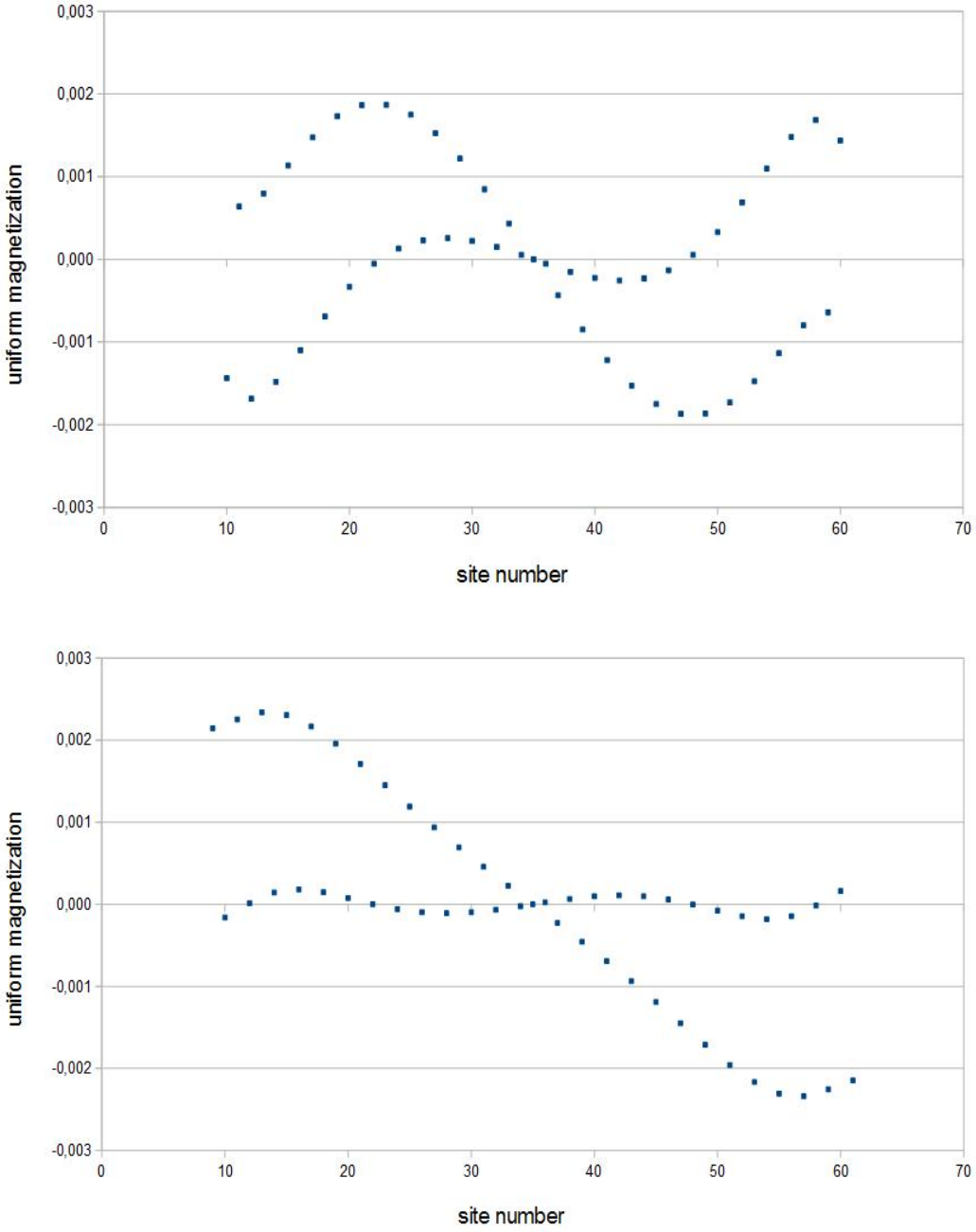

Figure 4.19: Uniform z-magnetization of the breather for a) $h = 0.1$ and b) $h = 0.2$. In both cases, two different curves are evident: one belongs to sites where j in eq. 4.8 is odd, the other to j even.

4.4 Time-evolution after a quench

In contrast to the early plans, it is not straightforward to predict how the breather might behave after a quench on the anisotropy; it is also hard to understand the structure of a quantum soliton: since it is a quantum object, it could be spread in the real space and not easy to see in its single-site magnetization or two-points correlators. The aim of this final section is to shed more light upon the quantum soliton behaviour and its aspect in real space.

The study is here carried out through time-dependent DMRG, a means that permits to prepare the system in one of its eigenstates and, then, make it evolve in time for a short lapse. The time-evolution of an eigenstate is trivial, but this tool gives the possibility to put the system out of equilibrium changing one or more parameters in the hamiltonian and then make it evolve following the laws of quantum mechanics.

Realizing a soliton state and then quenching the hamiltonian is a useful method to investigate in more detail the properties of this physical object. Two different kind of quenches have been realised, changing the external field magnitude or the anisotropy value. As for the first, the single-site z-magnetization behaviour has been observed for a sudden shift from $h = 0.2$ to $h = -0.1$ and vice versa (for $\Delta = 0.3$). The magnetization plot oscillates in time, as can be observed in Fig. 4.20. Moreover, the displacement between the magnetization at different sites remains constant during the time-evolution (Fig. 4.21).
Despite this, the uniform component always retains its shape and do not move (Fig. 4.22, while it should be reasonable to think that it should shift towards the other side of the chain, because of the change in sign of the field. As a consequence, it is the staggered part that moves: it substantially do not change its shape, but only shifts up or down (Fig. 4.23).
A quench from $h = 0.1$ to $h = 0.15$ has been also done (maintaining the field sign), and the physics is qualitatively the same.

As for the quench on the anisotropy, the behaviour of the soliton magnetization has been monitored after the change from $\Delta = -0.3$ to $\Delta = 0.3$ (with $h = 0.1$). The z-magnetization plot oscillates in time as before; in this case, however, the uniform magnetization shows a bump squashed on the right edge of the chain (Fig. 4.24). The reason is that, in this simulation, the starting point was the antiferromagnetic region, instead of the ferromagnetic one as before. Thus, in the antiferromagnetic region it seems that the bump feels more strongly the effect of the field. However, in this case too the bump never modifies in time.
The staggered magnetization shows a slightly different behaviour too. It shifts vertically, but also changes its shape (Fig. 4.25).
No other properties have been observed in depth, but the study should be continued considering two-points correlators. In this way, information about the extension of these excitations could be detected.

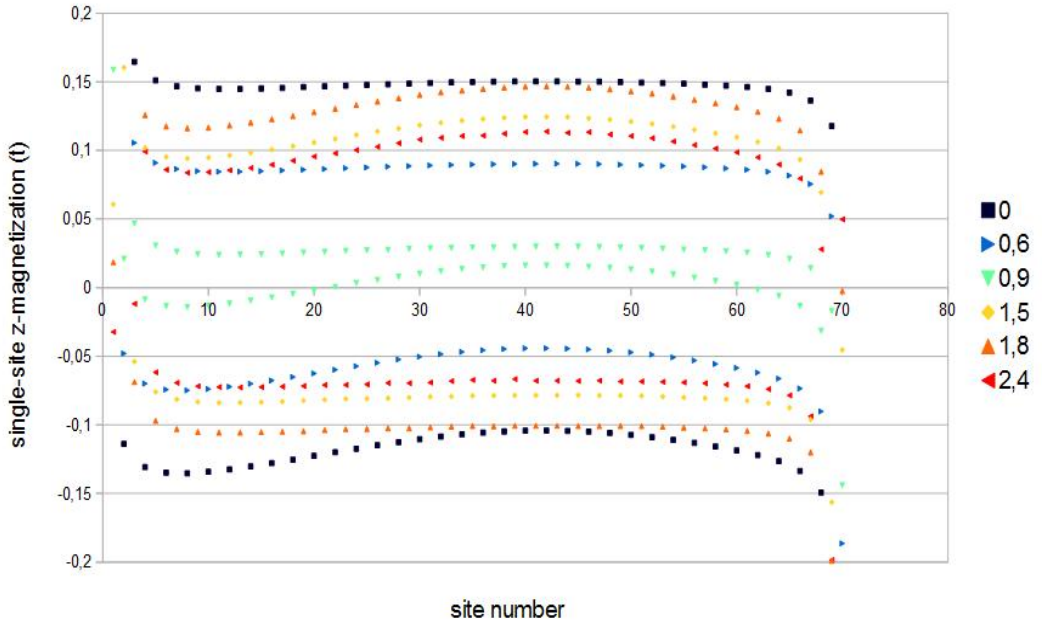

Figure 4.20: Single-site z-magnetization of the soliton after a quench from $h = 0.2$ to $h = -0.1$ (with $\Delta = 0.3$). The legend refers to the time after the quench: the magnetization oscillates in time.

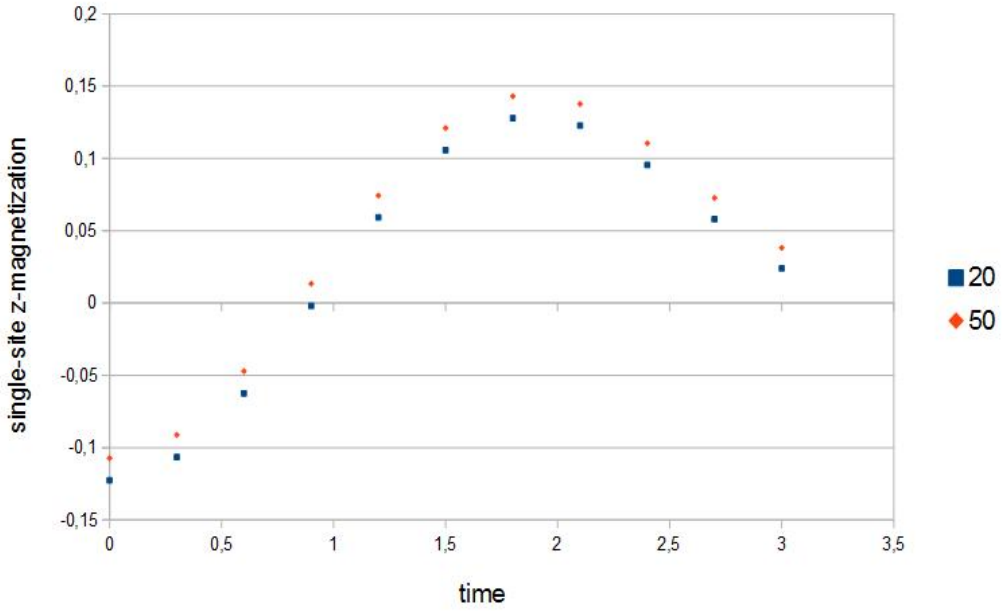

Figure 4.21: Single-site z-magnetization observed for sites number 20 (blue) and 50 (orange) fixed, as a function of time. A constant displacement can be noted.

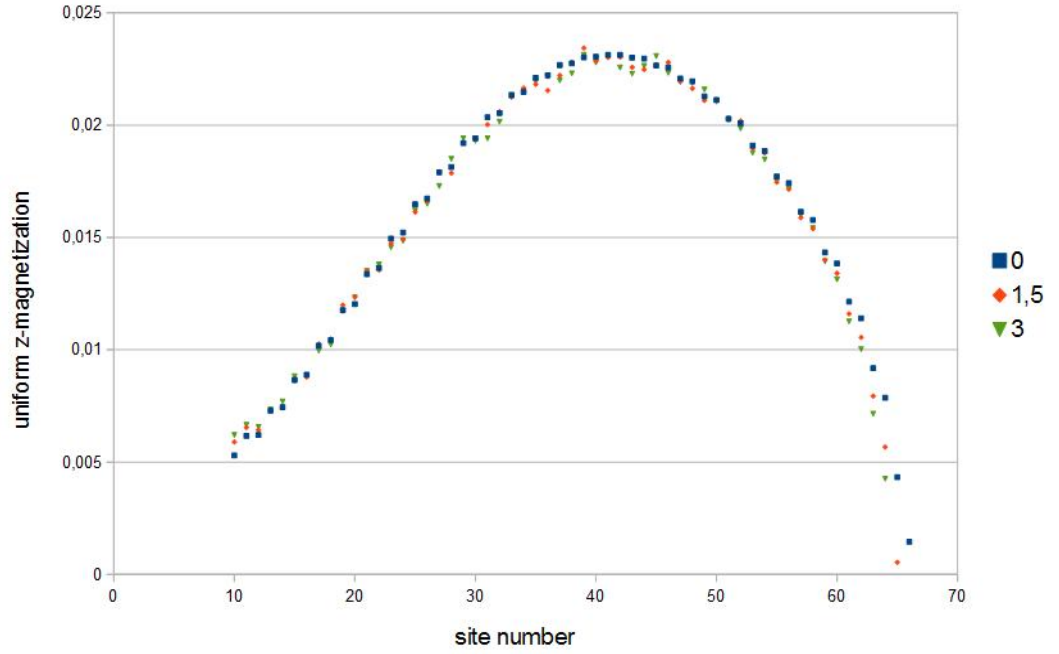

Figure 4.22: Uniform component referring to Fig. 4.20: it remains clearly stationary.

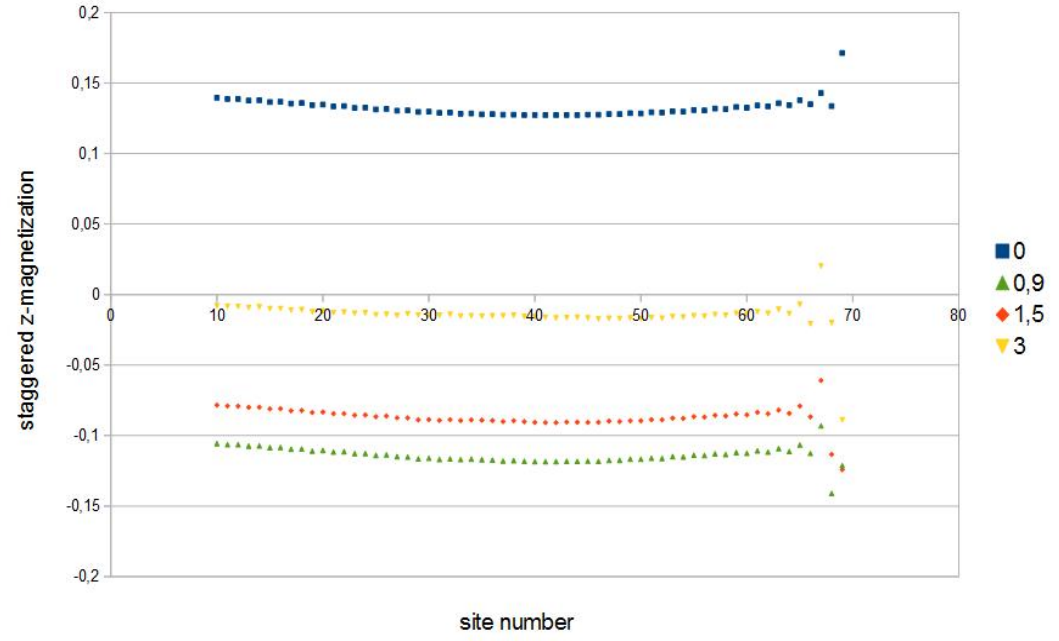

Figure 4.23: Staggered magnetization referring to Fig. 4.20: it shifts down and up, causing the oscillatory changes in the total magnetization.

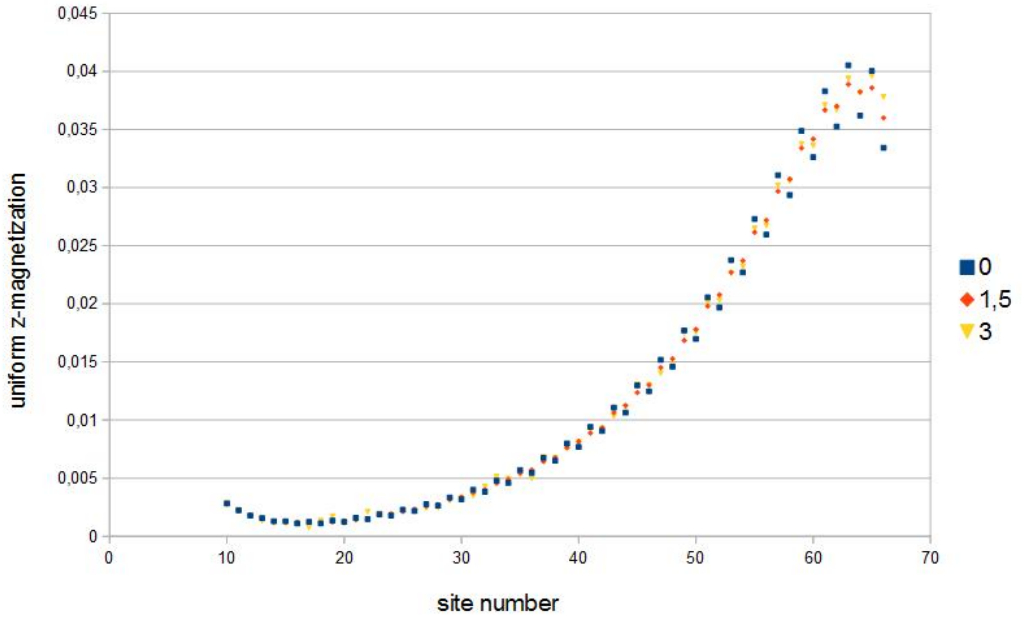

Figure 4.24: Uniform z-magnetization of the soliton after a quench on the anisotropy from $\Delta = -0.3$ to $\Delta = 0.3$.

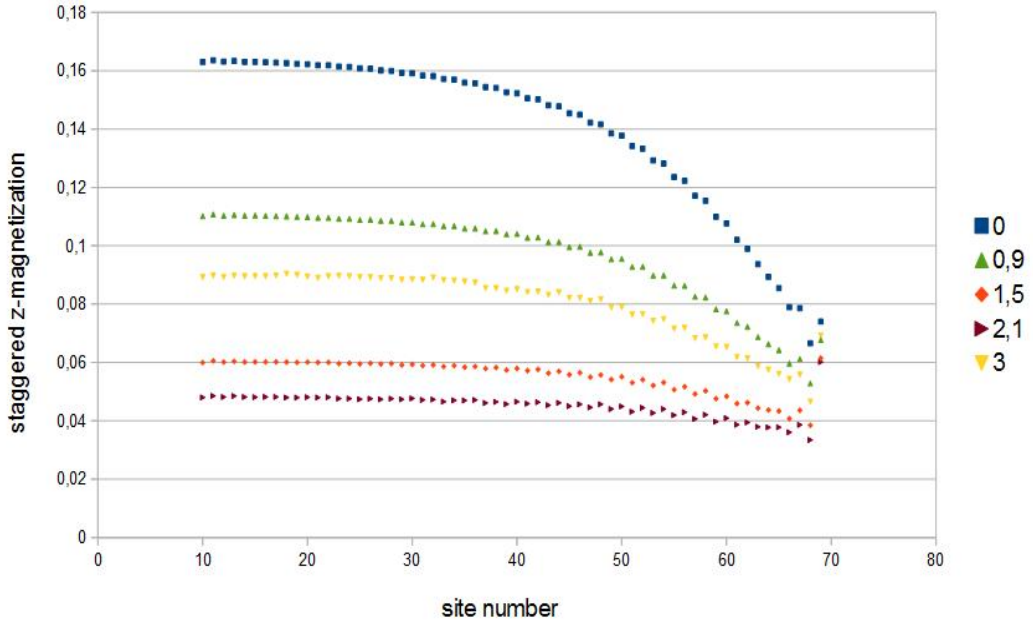

Figure 4.25: Staggered z-magnetization of the soliton after a quench on the anisotropy from $\Delta = -0.3$ to $\Delta = 0.3$.

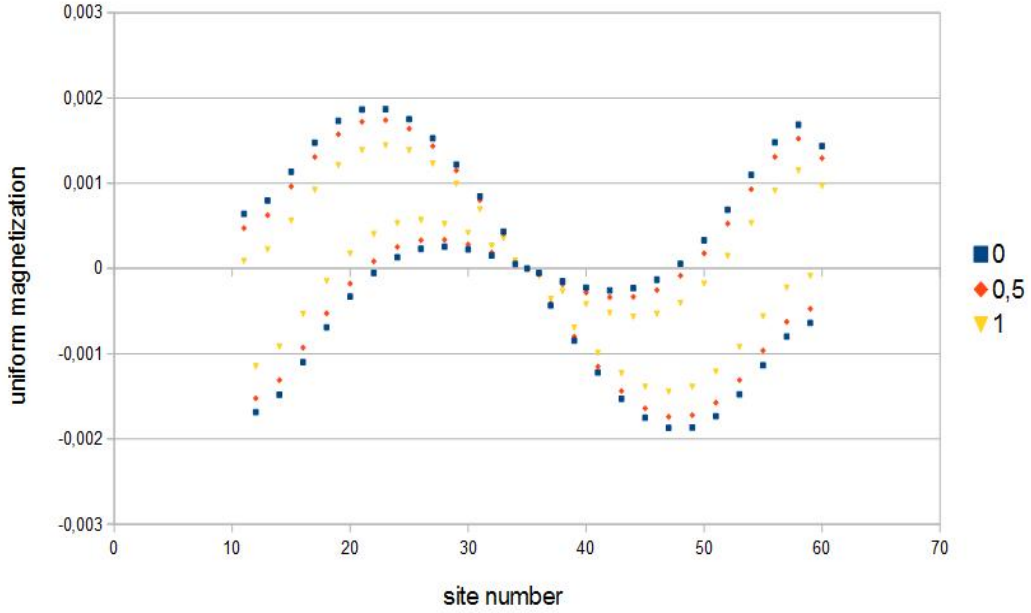

Figure 4.26: Uniform z-magnetization for the breather after a quench from $\Delta = -0.3$ to $\Delta = 0.3$ at different moments. Unlike the soliton case, it changes its shape with time.

In conclusion, it seems that the uniform component shape depends only on the chain length and the hamiltonian parameters; moreover, it never modifies after a quench. This suggests a sort of conservation law, due to a certain symmetry in the system. This symmetry might be the combination of both spin and field direction inversion: it is easy to see that it holds in the XXZ + h staggered hamiltonian. However, no evidence of this has been proved yet.

The breather properties have also been studied by means of quenches. In this case, the simulation has been done changing the anisotropy value from $\Delta = -0.3$ (where the breather exists and is stable) to $\Delta = 0.3$ (where it exists no more and is supposed to be described by solitons and antisolitons only).
As before the z-magnetization and its staggered component change with time; however, unlike the soliton case, also the uniform component modifies with time. This behaviour can be observed in Fig. 4.26. This is very peculiar but hard to interpret: it is better to understand in depth the soliton behaviour and, only then, try to explain the breather structure.
No further properties are evident from the single-site z-magnetization: the study should be continued considering two-points correlators also. They could bring further information about how correlations in the model change depending on different hamiltonian parameters.

Conclusions

The introduction of a staggered external magnetic field to the XXZ model strongly modifies its characteristics: as highlighted by the analytical analysis (even if exact for the XX + h staggered model only), the dispersion relation and the eigenstates have a much more complex form than without the field.
From the numerical study, it has been seen that this magnetic model follows the laws of the quantum sine-Gordon model predicted by the quantum field theory approach. First of all, this means that these predictions are valid; besides this, it confirms that the bosonization of the XXZ + h staggered model holds for the particular choice of hamiltonian parameters done.
Thus, the lowest soliton, antisoliton and breather energies have been pinpointed. Moreover, for $J = 1$ and $\Delta = \pm 0.3$, the breather has been found to exist in the antiferromagnetic point only.
Finally, the study of the soliton features has been started. Single-site z-magnetization yields interesting information, in particular from its uniform component. The bump never changes shape nor shifts after a quench. It does not move as for its classical counterpart, but this is not very surprising: these solitons are quantum objects, so they behave in a completely different way and cannot be thought in classical terms. Moreover, the fact that the bump depends only on the initial hamiltonian parameters and on the chain length suggests that there could be a sort of conservation law; the latter might derive from a symmetry in the model, such as the one obtained combining spin and field direction inversion.

This study helps in shining light upon the quantum solitons behaviour, but it is not conclusive. Instead, it is a starting point and there are several paths to follow to carry on with this research.
First of all, single-site z-magnetization is only the simplest observable one can use to determine soliton properties: a natural continuation of the study concerns the evaluation of two-points correlators, such as $S^z_j S^z_k$ and $S^+_j S^-_k$; they could provide further information about correlations in the system and how they change depending on different hamiltonian parameters.
On the other hand, solitons exist in principle even in the XX + h staggered model. As the latter has been solved exactly, all its energies and eigenstates are known. Starting from the assumption that the lowest-energetic solitons

are the first excited states in their own spin sectors, one can write the soliton and antisoliton eigenfunctions and study them.
This is harder than what may seem at first glance: $S_z = 0$ and $S_z = \pm 1$ correspond respectively to $N/2$ and $N/2 - 1$ spinless fermions in the energy bands of eq. 3.8. As a result, the eigenstate form will have $N/2$ and $N/2-1$ different coefficients in front of the states written in eq.s 3.19 and 3.21. Despite this is hard to write, it would probably brings helpful information about the soliton properties.

In conclusion, quantum solitons are really intriguing physical objects, and their behaviour has not been studied in depth yet. Their comprehension would probably bring to a better understanding of quantum mechanics itself and, perhaps, to the possibility of their employment in technology as quantum bits. However, there are several things to study yet: the hope is that this work might suggest further research in this topic.

Bibliography

[1] J. S. Russell, "Report on waves", "Fourteenth meeting of the British Association for the Advancement of Science", 1834

[2] J. Bundgaard, "A survey on the history and properties of solitons", lecture notes, 2011

[3] A.K. Liu, J.R. Holbrook, J.R. Apel, "Nonlinear internal wave evolution in the Sulu Sea", J. Phys. Oceanogr., 15, 1613-1624, (1985)

[4] P. S. Lomdahl, "What is a soliton?", Los Alamos Science, Spring 1984, pag. 27-31

[5] R. Rajaraman, "Solitons and Istantons", North-Holland, 1982

[6] J. E. Allen, "The Early History of Solitons (Solitary Waves)", IOPScience

[7] C. P. Burgess et al., "Bosonization in higher dimensions", Phys. Lett. B 336, 18-24 (1994)

[8] A.O. Gogolin et al., "Bosonization and strongly correlated systems", Cambridge University Press, 1998

[9] E. Fradkin, "Field theories of condensed matter systems", Cambridge University Press, 1991

[10] E. Miranda, "Introduction to bosonization", Braz. Jour. of Phys., vol. 33, no. 1, March, 2003

[11] J. von Delft, H. Schoeller, "Bosonization for Beginners — Refermionization for Experts" Annalen Phys. 7 225-305 (1998)

[12] H. Bethe "On the theory of metals. Eigenvalues and eigenfunctions of the linear atom chain", Zeitschrift fr Physik, 71:205226 (1931)

[13] M. Takahashi, "Thermodynamics of One-Dimensional Solvable Models", Cambridge University Press, 1999

[14] M. Karbach and G. Muller, "Introduction to the Bethe ansatz I", arXiv:cond-mat/9809162 v1 10 Sep 1998

[15] F. Franchini, "Notes on Bethe ansatz techniques", 2011

[16] A. Zamolodchikov, Int. J. Mod. Phys. A 10 (1995) 1125

[17] S. Lukyanov and A. Zamolodchikov, Nuclear Physics B 493 (3), 571-587

[18] M. Henkel, "Conformal Invariance and Critical Phenomena", Springer, 1999

[19] F. Ravanini, "Finite size Effects in Integrable Quantum Field Theories", 2001

[20] U. Schollwock, "The density-matrix renormalization group", Rev. Mod. Phys., vol. 77, January 2005

[21] U. Schollwock, S. R. White, "Methods for Time Dependence in DMRG", arXiv, May 2006